Analytical Biochemistry 640 (2022) 114455

Contents lists available at ScienceDirect

Analytical Biochemistry

journal homepage: www.elsevier.com/locate/yabio

High affinity human Fc specific monoclonal antibodies for capture kinetic analyses of antibody-antigen interactions

Vishal Kamat *, Candice Boutot, Ashique Rafique, Christian Granados, Jing Wang, Ashok Badithe, Marcela Torres, Ishita Chatterjee, Olav Olsen, William Olson, Tammy Huang

Therapeutic Proteins, Regeneron Pharmaceuticals, USA

ARTICLE INFO

Keywords:
Label-free optical biosensor
Monoclonal antibody
Anti-human Fc
Capture kinetics
Immunoassay

ABSTRACT

We recently demonstrated that capturing human monoclonal antibodies (hmAbs) using high affinity anti-human Fc (AHC) antibodies allows reliable characterization of antibody-antigen interactions. Here, we characterized six human Fc specific mouse monoclonal antibodies (mAbs) and compared their binding profiles with three previously characterized goat AHC polyclonal antibodies (pAbs), exhibiting properties of a good capture reagent. All six mouse AHC mAbs specifically bound with high affinity to the Fc region of hIgG1, hIgG2, hIgG4 and to 43 different hIgG variants, containing substitutions and/or mutations in the hinge and/or Fc region, that have been reported to exhibit modified antibody effector function and/or pharmacokinetics. Biacore sensor surfaces individually derivatized with mouse AHC mAbs exhibited >2.5-fold higher hIgG binding capacity compared to the three goat AHC pAb surfaces and reproducibly captured hIgG over 300 capture-regeneration cycles. The results of the capture kinetic analyses performed on 31 antibody-antigen interactions using surfaces derivatized with either of the two highest affinity AHC mAbs (REGN7942 or REGN7943) were in concordance with those performed using goat AHC pAb surfaces. Our data demonstrate that AHC mAbs such as REGN7942 and REGN7943 that have properties superior than the three goat AHC pAbs are highly valuable research reagents, especially to perform capture kinetic analyses of antibody-antigen interactions on optical biosensors.

1. Introduction

Technological advances in the discovery and development of monoclonal antibodies (mAbs) have enabled their expanded use in novel applications across diverse fields, including biochemistry, molecular and cellular biology and diagnostics. Among different areas, the healthcare sector has perhaps benefited the most owing to the development of multiple methods for producing fully human mAbs (hmAbs) and IgG variants for their optimized use as therapeutic agents [1–8]. Currently, more than 120 therapeutic mAbs have been approved for a wide range of diseases and generated over $130 billion in global revenue in 2019 [9].

Therapeutic mAb discovery and development is an extremely complex, arduous, and multi-step process requiring collaborative efforts across multidisciplinary teams. As part of the initial screening efforts, a variety of high-throughput biophysical, biochemical and cell-based assays are employed to narrow down the number of candidates to a small subset of potential therapeutic mAbs, which later undergo a rigorous secondary screening process. The kinetics of antigen (Ag) binding to mAbs are among the most important properties considered during the selection of lead therapeutic candidate. Therefore, it is essential that the measured association rate constant (k_a), dissociation rate constant (k_d), and equilibrium dissociation constant (K_D) of mAbs binding to Ags are reliable and reproducible. Capture kinetic assay allows rapid determination of binding kinetic parameters of mAb-Ag interactions and is routinely performed on a wide range of label-free optical biosensors. In this assay, a tag-specific capture reagent is covalently immobilized onto the sensor surface to capture the ligand (interacting partner attached to the surface) in a specific orientation and varying concentrations of analyte (interacting partner that is passed in solution over the ligand surface) are injected over the ligand-captured surface. The reliability of results from such assays largely depends on

; SPR, Surface Plasmon Resonance; mAb, Monoclonal antibody; Ag, Antigen; pAb, Polyclonal antibody; AHC, anti-human Fc; k_a, Association rate constant; k_d, Dissociation rate constant; K_D, Equilibrium dissociation constant; $t_{½}$, Dissociative half-life; hmAb, Human monoclonal antibody; KinExA, Kinetic exclusion assay; NHP, Non-human primate.

* Corresponding author.
E-mail address: vishal.kamat@regeneron.com (V. Kamat).

https://doi.org/10.1016/j.ab.2021.114455
Received 12 August 2021; Received in revised form 5 November 2021; Accepted 8 November 2021
Available online 14 November 2021

the quality of capture reagents used and selection of an imperfect capture reagent can have profound effects on the measured k_a, k_d, and K_D values [10]. For reliable kinetic measurements of hmAb-Ag interactions, AHC capture reagent should exhibit several key properties that include: (i) high binding activity following immobilization onto the sensor surface; (ii) ability to capture mAb at low concentrations to enable kinetic screening of unpurified mAbs from conditioned media (CM); (iii) forms a stable complex with the captured mAb with minimal baseline drift; (iv) a hIgG binding affinity that is agnostic to hIgG subclass; (v) a binding profile that is minimally affected by analysis temperature and buffer conditions; (vi) withstand multiple regeneration cycles over a range of analysis temperatures and buffer conditions without losing its binding activity [11].

Recently, we showed that although Protein A, Protein G, Protein A/G, and a commercial mouse anti-human Fc (AHC) mAb exhibited many properties of a good capture reagent, the capture kinetic analyses performed on these derivatized surfaces yielded erroneous k_a, k_d, and K_D values [10]. The K_D values measured using Protein A, Protein G, and Protein A/G surfaces were up to 2800-fold weaker than those determined using a solution based kinetic exclusion assay (KinExA), while the commercial mouse AHC mAb surface generated binding affinities that were up to 14-17-fold weaker compared to those measured using the three different goat AHC polyclonal antibody (pAb) surfaces. Upon further investigation, we discovered that all three goat AHC pAbs bound to human mAb (hmAb) with sub-nanomolar affinity, while the mouse AHC mAb had a weaker affinity for human IgG (hIgG) with $t_{½}$ values ranging from 1.4 to 3.3 min. Our study showcased that a high affinity Fc specific antibody, with $t_{½}$ values similar to or better than the goat AHC pAbs (11 min), is a desirable capture reagent for performing capture kinetic analyses of hmAbs using real time optical biosensor.

In this study, we report the characterization of six new mouse AHC mAbs for their application as capture reagents to determine hmAb-Ag interactions on label-free optical biosensors. These six AHC mAbs were identified based on their specificity to the Fc region of hIgG and lack of cross-reactivity to cynomolgus monkey IgG. Details of the six mouse AHC mAbs are provided in Table 1. The three commercial goat AHC pAbs which were previously shown to have properties of a good AHC capture reagent to characterize mAb-Ag interaction on a label-free biosensor [10], were also included in the current study as benchmark comparators. We first assessed the binding specificity of these six mouse AHC mAbs to the Fc region of hIgG and later measured their binding affinity to the three hIgG subclasses (hIgG1, hIgG2, hIgG4) and 43 different hIgG variants, commonly reported in the literature with substitutions and/or mutations in the hinge and/or Fc region of hIgG for modified antibody effector function and pharmacokinetics. Once immobilized onto a CM5, CM4 and C1 sensor chip, the two highest affinity mouse AHC mAbs (REGN7942 and REGN7943) were further assessed for their long-term capture stability (10,000 s) of hIgG1 and hIgG4 with a S228P substitution ($IgG4^P$) that reconstructs the human IgG1 hinge sequence (CPPC) to promote stabilization of disulfide bonds between the 2 heavy chains. Their performance in capture kinetic analyses of 31 high affinity hmAb-Ag interactions was also evaluated. Our work demonstrates that AHC mAbs with binding profiles similar to REGN7942 and REGN7943 can be valuable research reagents to develop a wide range of immunoassays such as the capture reagents for the reliable characterization of mAb-Ag interactions.

Table 1
Details of six mouse AHC mAbs.

Mouse AHC mAb	Mouse IgG Subclass
REGN2567	IgG1
REGN2681	IgG1
REGN7779	IgG1
REGN7941	IgG2a
REGN7942	IgG2a
REGN7943	IgG2a

2. Materials and methods

2.1. Reagents

N-(3-dimethylaminopropyl)-*N*-ethylcarbodiimide (EDC), *N*-hydroxysuccinimide (NHS), ethanolamine–HCl (Catalog# BR100633), rabbit anti-mouse antibody (Catalog# BR100838), CM5 sensor chips (Catalog# BR100530), CM4 sensor chips (Catalog# BR100534) and C1 sensor chips (Catalog# BR100535) were purchased from Cytiva (formerly GE Healthcare Life Sciences). Sodium acetate, pH 5.0 was purchased from Ricca Chemical (Catalog# 61–1). HEPES (Teknova, Catalog# H1035), NaCl (Gibco, Catalog# 24740–011), EDTA (BDH Chemicals, Catalog# BDH8730-1) and Tween-20® (Bio-Rad, Catalog# 161–0781) were used to prepare the running buffer. Different AHC pAbs were purchased from Jackson ImmunoResearch (Catalog# 109-005-098), MP Biomedicals (Catalog# 0855071) and Southern Biotech (Catalog# 2048–01).

REGN2567 and REGN2681 were recombinantly produced using stable Chinese hamster ovary (CHO) cell lines while the remaining four mouse AHC mAbs were produced using the hybridoma clones. The hmAbs and Ags used in this study were recombinantly expressed using stable CHO cell lines. All Ags were expressed with a C-terminal myc-myc-hexahistidine tag with a GG linker between the myc tags (EQKLISEEDLGGEQKLISEEDLHHHHHH). The Ags were first purified by immobilized metal chelate affinity chromatography (IMAC) column; using either zinc charged iminodiacetic acid (IDA) resin or cobalt charged TALON resin and the monomeric Ag species were later purified by size exclusion chromatography (SEC). The hmAbs and the six mouse AHC mAbs were first purified using Protein A resin affinity column followed by SEC. The concentration of all the reagents were determined by measuring their absorbances at 280 nm and their predicted extinction coefficients (based on their amino acid sequence) and were later stored at −80°C until used.

2.2. Instrumentation

All the real time binding data were generated on the surface plasmon resonance (SPR) based Biacore 8 k (Cytiva, formerly GE Healthcare Life Sciences) optical biosensor.

2.3. Generation of mouse AHC mAb

All six mouse AHC mAbs were generated by immunizing wild-type Balb/c mice with the Fc region of hIgG4 with S228P, H435R, Y436F, L445P substitutions. The spleens were later harvested and fused to mouse myeloma cells to produce hybridoma clones. The supernatants of the hybridoma clones were later screened for their binding affinity to hIgG1 and hIgG4 subclasses and cross-reactivity to cynomolgus monkey IgG.

2.4. Determination of binding specificity of different AHC antibodies using ELISA

Flat bottom 96-well microtiter plates (Thermo Scientific, # 15041) were coated overnight at 4°C with 0.5 μg/mL of IgG from different species, Fab region of either hIgG1 (hFab_1) or hIgG4 (hFab_4),prepared in PBS buffer (Irvine Scientific, # 9236). The plates were rinsed thrice with wash buffer (PBS containing 0.05% Tween-20) and blocked for 1 h at room temperature (RT) in blocking buffer (PBS containing 0.5% BSA). The binding of six mouse AHC mAbs and three goat AHC pAbs from Jackson ImmunoResearch (subsequently referred as goat AHC pAb-1), MP Biomedicals (subsequently referred as goat AHC pAb-2) and Southern Biotech (subsequently referred as goat AHC pAb-3) was later tested (in duplicate) at an 11-point, three-fold serial dilution from 20 nM to 0.34 pM prepared in blocking buffer. The antibody concentrations

used in both ELISA and SPR assays were calculated based on the whole IgG molecule and not on their bivalency. Coat-specific positive control antibodies (details provided in Supplementary Table 1) and buffer only controls were also included. After 1 h incubation at RT, ELISA plates were washed thrice with wash buffer and horseradish peroxidase (HRP) conjugated goat anti-mouse Fcγ specific antibody (Jackson ImmunoResearch, # 115-035-164) or bovine anti-goat IgG antibody (Jackson ImmunoResearch # 805-035-180) was added at 1:5000 dilution in blocking buffer. After 1 h incubation at RT, the plates were rinsed thrice with wash buffer and AHC antibody binding was determined using the colorimetric HRP-substrate, 3,3′,5,5′-tetramethylbenzidine (TMB colorimetric substrates A and B, BD Biosciences # 51-2606 KC and # 51-2607 KC, respectively) following the manufacturer's recommended protocol. The absorbance at 450 nm for each well was recorded using ENVISION multimode plate reader (PerkinElmer, # 2105) and the dose-dependent AHC antibody binding was analyzed using a 4-parameter logistic (4PL) curve model and the EC_{50} values were calculated using GraphPad Prism software v9.0.

2.5. Binding studies performed on SPR biosensor

Unless otherwise specified, all binding studies were performed in freshly prepared, filtered and degassed running buffer containing 10 mM HEPES, 150 mM NaCl, 3 mM EDTA, 0.05% Tween-20 (HBS-ET) at 25°C. Different AHC capture molecules were immobilized onto the CM5, CM4 or C1 sensor surface using the standard EDC/NHS chemistry reported earlier [10]. After the activation of the sensor surface by injecting a 1:1 (v/v) mixture of 400 mM EDC and 100 mM NHS for 10 min, different capture reagents (20–25 μg/mL) prepared in 10 mM sodium acetate, pH 5.0 were injected for 6–10 min followed by a 6 min injection of 1 M ethanolamine, pH 8.5.

The kinetics of AHC antibodies for binding to hIgG subclasses or different hIgG variants with substitutions and/or mutations in the Fc and/or hinge region were studied by first capturing very low density (3–7 RU) of goat AHC pAb or mouse AHC mAb over a CM5 sensor surface immobilized with either a mouse anti-goat Fc mAb (Southern Biotech, Catalog# 6158–01) or a rabbit anti-mouse Fc pAb (Cytiva, formerly GE Healthcare Life Sciences, Catalog# BR100838), respectively. Different concentrations of hIgG (wild-type or different variants), diluted by three-fold in HBS-ET running buffer were later injected for 3min and the dissociation of the bound hIgG from the captured AHC antibodies was monitored for 20 min. At the end of each cycle, the captured AHC antibody surfaces were regenerated using the conditions provided in Supplementary Table 2.

The binding capacity of different AHC antibody surfaces was assessed on a CM5, CM4 and C1 sensor chip by injecting different concentrations of hIgG1, hIgG2, hIgG4, or $hIgG4^P$ (0.1, 0.5, 2, 10 μg/mL) for 3 min followed by a 10 min dissociation phase. At the end of each cycle, the AHC antibody surfaces were regenerated using the conditions provided in Supplementary Table 2. The reproducibility of the hIgG capture level was tested by capturing 600–650 RU of hIgG1, hIgG2, hIgG4 or $hIgG4^P$ over the six different mouse AHC mAbs, individually immobilized on a CM5 sensor surface followed by the surface regeneration using a 4 s injection of 20 mM phosphoric acid. The capture-regeneration steps were repeated for more than 300 times at 37°C. The long term capture stability was assessed by capturing hIgG1 or $hIgG4^P$ on a CM5, CM4 and C1 sensor chip, individually immobilized with the three goat AHC pAbs, REGN7942 and REGN7943 using an "analyte" injection command with a 10,000 s (2hr and 47 min) dissociation phase.

The kinetics of the hmAb binding to its respective Ag were studied on a CM5 sensor chip individually immobilized with the three goat AHC pAbs, REGN7942 and REGN7943. The hmAbs were first captured over different AHC capture surfaces followed by the injection of different concentrations of specific Ag (three-fold serial dilution) for 3 min. The dissociation of bound Ag from the captured hmAbs was monitored for either 15 min or 1 h in the HBS-ET running buffer. At the end of each cycle, the capture surfaces were regenerated using the conditions provided in Supplementary Table 2.

2.6. SPR data processing and analysis

The real-time binding data were first double reference subtracted using the Biacore Insight Evaluation software, version 2.0 (Cytiva, formerly GE Healthcare Life Sciences) and were later fit using a 1:1 binding model with mass transport limitation either using the Biacore Insight Evaluation software, or using the Scrubber software (version 2.0c, BioLogic Software, Campbell, Australia).

3. Results

3.1. All six mouse AHC mAbs specifically bound to the Fc region of human IgG

The constant regions of human and monkey IgG share more than 90% sequence homology and hence AHC mAbs that specifically bind the Fc region of hIgG are critical reagents in the biopharmaceutical industry, especially for analyzing pharmacokinetic (PK) and pharmacodynamic (PD) studies performed in non-human primates (NHP). We therefore first assessed binding specificity of all six in-house generated mouse AHC mAbs by testing their binding to the hFab_1, hFab_4, rabbit IgG and NHP IgG – cynomolgus monkey IgG and rhesus monkey IgG. The binding ELISA studies were performed on a 96-well microtiter plate at RT and the results of concentration dependent binding of different antibodies are shown in Fig. 1 while their respective EC_{50} values are reported in Table 2. All three goat AHC pAbs bound to the Fc region of hIgG with EC_{50} values ranging from 46.8–102 pM, but also showed binding to IgG of cynomolgus monkey, rhesus monkey and rabbit with EC_{50} values ranging from 80–112 pM, 88–124 pM and 270–600 pM, respectively. Weak binding to hFab_1 and hFab_4 was also observed at 20 nM of goat AHC pAb-1 and goat AHC pAb-2 but not for goat AHC pAb-3. In contrast, all six mouse AHC mAbs were very specific to the Fc region of hIgG with EC_{50} values ranging from 28–109 pM. No detectable binding was observed to hFab_1, hFab_4, cynomolgus monkey IgG, rhesus monkey IgG and rabbit IgG. Among the six mouse AHC mAbs, REGN2567 and REGN2681 showed highest binding affinity with EC_{50} of 27–34 pM while REGN7941, REGN7942, and REGN7943 exhibited weakest affinity with EC_{50} values ranging from 81–109 pM.

3.2. All six mouse AHC mAbs bound to human IgG with high affinity

The binding affinities of six mouse AHC mAbs to different hIgG subclasses (hIgG1, hIgG2, and hIgG4) were next determined and their binding kinetic parameters were compared with those measured for the three commercial goat AHC pAbs [10]. To minimize avidity-driven binding that can be caused due to bivalent analytes (dimerized Fc region of hIgG) and to ensure that the measured affinities are a better representation of a true 1:1 binding, capture kinetic studies were performed using a very low density AHC antibody capture surface (3–7 RU). Each goat AHC pAb or mouse AHC mAb was individually captured on sensor surfaces immobilized with mouse anti-goat Fc mAb or rabbit anti-mouse Fc pAb, respectively. Different concentrations of hIgG1, hIgG2, or hIgG4 were subsequently injected (as analyte) for 3 min and the dissociation of the bound hIgG was monitored for 20 min. The real time binding sensorgrams (black lines) along with the global fits (red lines) are shown in Fig. 2 and the results of the kinetic analyses are provided in Table 3.

As reported previously [10], all three goat AHC pAbs showed biphasic dissociation curves and the largest biphasic dissociation was observed for hIgG4 binding. This was not surprising since we would expect that the polyclonal nature of goat AHC pAbs would bind hIgG with diverse binding affinities. Moreover, it is important to understand that even at such low density surfaces, it could be difficult to generate

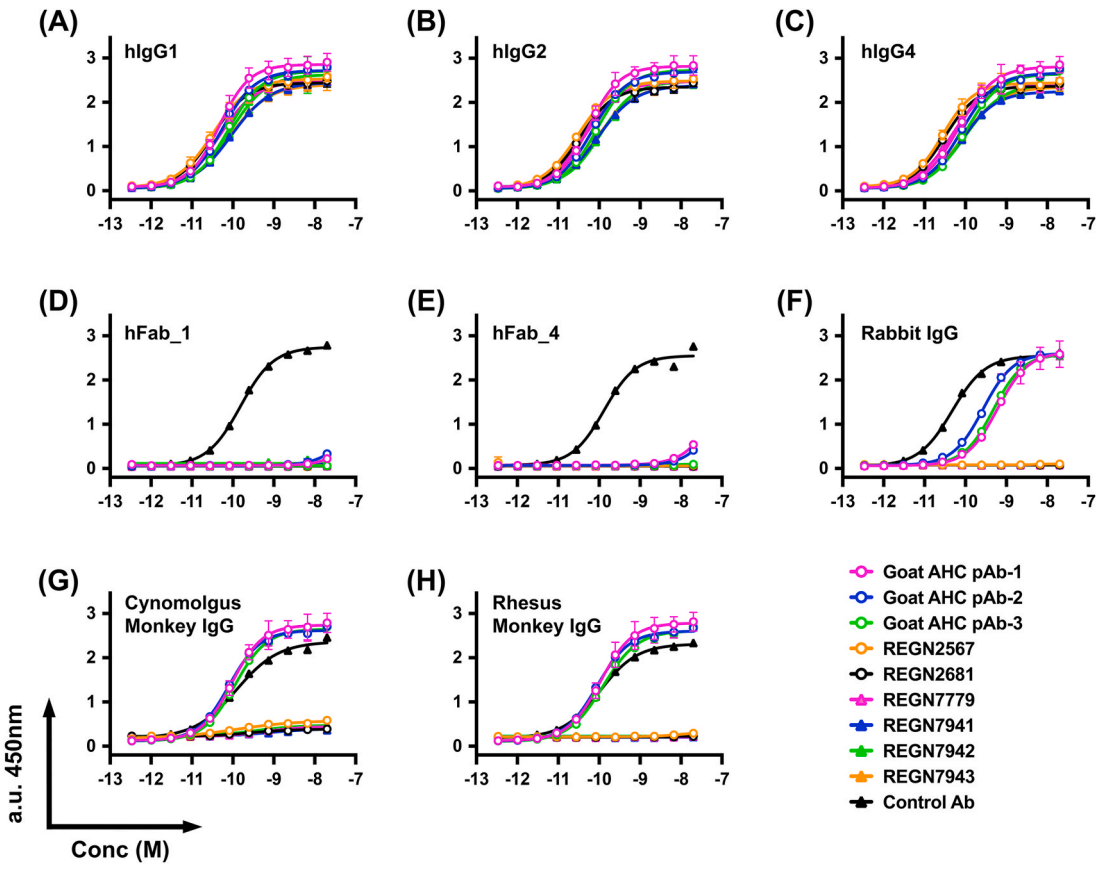

Fig. 1. Binding specificity of different AHC antibodies to purified immunoglobulin using ELISA. The ELISA plates were first coated overnight at 4°C with 0.5 μg/mL of (**A**) hIgG1, (**B**) hIgG2, (**C**) hIgG4, (**D**) hFab_1, (**E**) hFab_4, (**F**) rabbit IgG, (**G**) cynomologous monkey IgG, or (**H**) rhesus monkey IgG. After three washes in wash buffer, the plates were blocked with blocking buffer for 1 h. The wells were later incubated with varying concentrations of AHC antibodies for 1 h and after washing thrice in wash buffer, the wells were incubated with HRP conjugated goat anti-mouse Fc antibody or bovine anti-goat IgG antibody and finally processed for enzymatic reaction for the detection of bound AHC antibodies. For each IgG coat, control antibody (black triangle) was used as positive control and the concentration dependent binding of goat AHC pAb-1 (magenta circle), goat AHC pAb-2 (blue circle), goat AHC pAb-3 (green circle), REGN2567 (orange circle), REGN2681 (black circle), REGN7779 (magenta triangle), REGN7941 (blue triangle), REGN7942 (green triangle), or REGN7943 (orange triangle) to different purified immunoglobulins are shown. Each data point represents the average of duplicate samples for each concentration ± standard deviation. (For interpretation of the references to color in this figure legend, the reader is referred to the Web version of this article.)

Table 2
Summary of binding specificity of nine AHC antibodies and their cross-reactivity to immunoglobin from different animal species by ELISA.

	Coated Surface							
AHC Antibody	**hIgG1**	**hIgG2**	**hIgG4**	**hFab_1**	**hFab_4**	**Cynomolgus Monkey IgG**	**Rhesus Monkey IgG**	**Rabbit IgG**
Goat AHC pAb-1	4.68E-11	5.61E-11	6.91E-11	>20 nM	>20 nM	9.47E-11	1.06E-10	6.06E-10
Goat AHC pAb-2	5.38E-11	6.86E-11	7.96E-11	>20 nM	>20 nM	8.04E-11	8.86E-11	2.68E-10
Goat AHC pAb-3	7.74E-11	8.75E-11	1.02E-10	NB	NB	1.12E-10	1.24E-10	4.80E-10
REGN2567	3.28E-11	3.03E-11	2.76E-11	NB	NB	NB	NB	NB
REGN2681	3.20E-11	3.36E-11	3.10E-11	NB	NB	NB	NB	NB
REGN7779	4.87E-11	4.54E-11	4.45E-11	NB	NB	NB	NB	NB
REGN7941	9.08E-11	9.33E-11	8.15E-11	NB	NB	NB	NB	NB
REGN7942	8.79E-11	1.09E-10	9.92E-11	NB	NB	NB	NB	NB
REGN7943	8.31E-11	9.09E-11	8.57E-11	NB	NB	NB	NB	NB
Control Ab				1.52E-10	1.31E-10	1.22E-10	1.04E-10	4.73E-11

Values reported in the table represent EC_{50} values (in Molar) derived by fitting the dose-dependent binding of different AHC antibodies or coat-specific control antibodies using a using a 4-parameter logistic (4PL) curve model using GraphPad Prism software v9.0.
NB represents no binding was observed under the current experimental conditions.

binding data which are devoid of any avidity-driven binding of a dimeric analyte (hIgG) to a dimeric ligand (AHC antibodies); more pronounced during the latter part of the dissociation phase. Therefore, k_d values were determined by fitting the initial 3–7 min of the dissociation phase and the association phase was later fitted to calculate the k_a and K_D values. However, there is one caveat with our data analysis. Unlike the dissociation phase wherein the change in the binding response is only influenced by analyte dissociation, the binding sensorgrams observed in the association phase is the result of both association and dissociation processes. Therefore, selection of only the initial fast dissociation phase would theoretically ignore the contribution of the slower off-rate during k_a calculation. However, we believe that adopting such curve fitting strategy is the best possible alternative to determine an apparent binding affinity that closely represents the true 1:1 binding affinity and as a

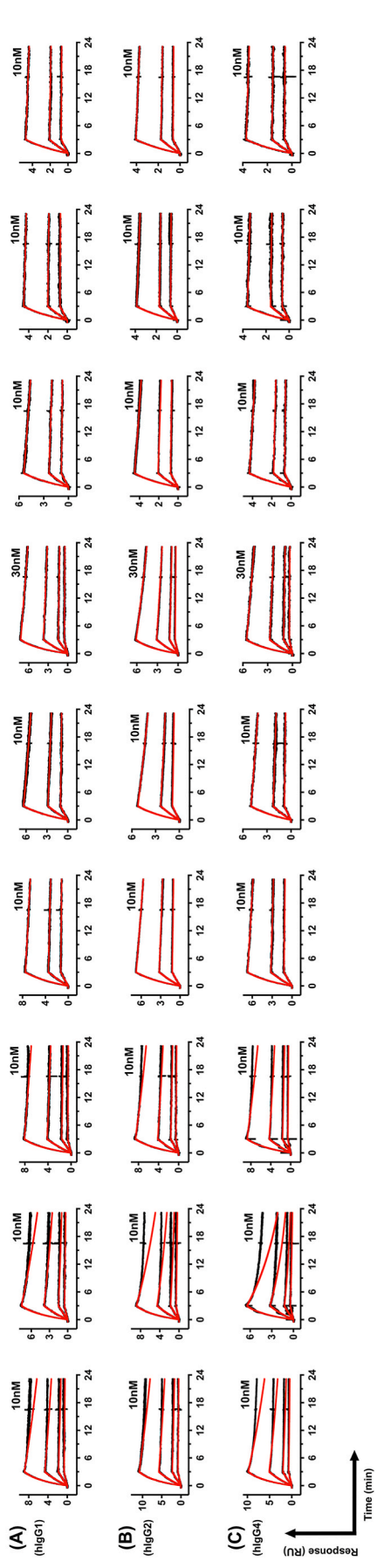

Fig. 2. Binding of different AHC antibodies to wild-type hIgG subclasses. Different goat AHC pAbs or mouse AHC mAbs were captured at a very low density (3–7 RU) using mouse anti-goat Fc mAb or rabbit anti-mouse Fc pAb, respectively. Different concentrations of (**A**) hIgG1, (**B**) hIgG2, or (**C**) hIgG4 (serially diluted by three-fold) were subsequently injected for 3 min followed by a 20 min dissociation time. The real time binding sensorgrams (shown in black) represent duplicate injections for each hIgG concentration, while the fits generated by globally fitting the data using 1:1 binding model with mass transport limitation are shown as red lines. The highest hIgG concentration used to fit the data is also provided and the results of the kinetics analyses is listed in Table 3. (For interpretation of the references to color in this figure legend, the reader is referred to the Web version of this article.)

result would allow affinity ranking of different AHC antibodies included in the study.

Goat AHC pAb-1 and pAb-3 bound to hIgG2 and hIgG4 with similar binding kinetics (K_D and $t_{½}$ values ranging from 262–426 pM and 30–50 min, respectively). However, goat AHC pAb-3 bound to hIgG1 with approximately 2.3-fold higher affinity and exhibited a 2.7-fold slower dissociation rate than goat AHC pAb-1. Goat AHC pAb-1 and pAb-2 bound to hIgG1 with similar binding kinetics, but the dissociation rates of goat AHC pAb-2 for hIgG2 and hIgG4 was observed to be approximately two-fold faster than that measured for goat AHC pAb-1. In contrast, monophasic dissociation was observed for all six mouse AHC mAbs and they bound to hIgG1, hIgG2, and hIgG4 with sub-nanomolar affinities. Less than a two-fold difference in the K_D values was measured for all six mouse AHC mAbs binding to the different hIgG subclasses tested. REGN7779 bound with the weakest affinity (K_D and $t_{½}$ values ranging from 471–850 pM and 48–85 min, respectively), followed by REGN2681 (K_D values ranging from 269–408 pM and 50–78 min, respectively). REGN2567 and REGN7941 bound with comparable binding affinities with K_D values ranging from 157–216 pM and 326–371 pM and $t_{½}$ values ranging from 78–114 min and 84–96 min, respectively. The highest affinity mAbs, REGN7942 and REGN7943, bound with similar binding kinetics and their K_D values ranged from 88–134 pM and 110–154 pM, respectively (Table 3). The dissociation rates for REGN7942 and REGN7943 were also the slowest among the six mouse AHC mAbs with $t_{½}$ values ranging from 160–237 min and 155–207 min, respectively.

3.3. All six mouse AHC mAbs bound to 43 different hIgG variants with high affinity

Modification of the Fc region of hIgG with different substitutions and/or mutations has enabled researchers to generate bispecific antibodies (bsAbs) and novel therapeutic modalities with modified antibody effector functions such as antibody-dependent cellular cytotoxicity (ADCC), antibody-dependent cell-mediated phagocytosis (ADCP), complement-dependent cytotoxicity (CDC), FcRn-mediated IgG homeostasis, efficient antigen presentation to dendritic cells and altered PK/PD properties [12–35]. To assess whether previously reported IgG modifications influence the binding of any of the six mouse AHC mAbs reported in this study, a total of 43 different hIgG variants, with substitutions and/or mutations in the hinge and/or Fc region, individually or in combination were generated (Table 4) and their binding to different AHC antibodies was examined. The results of the kinetic analyses of nine AHC antibodies (three goat AHC pAbs and six mouse AHC mAbs) binding to selective hIgG variants are provided in Table 3 and their respective real time binding sensorgrams (black lines) along with the global fits (red lines) are shown in Fig. 3. The k_a, k_d, K_D, and $t_{½}$ values for the complete set of 46 hIgGs (3 wild-type and 43 variants) are shown in a scatter plot in Fig. 4 and their kinetic values are reported in Supplementary Table 3.

Between the three goat AHC pAbs tested, the goat AHC pAb-2 exhibited the weakest binding affinity to the different hIgG variants (K_D and $t_{½}$ values ranging from 145 pM–1.3 nM and 11–52 min, respectively). The goat AHC pAb-3 bound with the highest affinity (K_D and $t_{½}$ values ranging from 59–540 pM and 31–168 min, respectively), while the goat AHC pAb-1 bound to different hIgG variants with K_D and $t_{½}$ values ranging from 95–930 pM and 18–68 min, respectively.

Among the six mouse AHC mAbs, REGN2681, REGN7779 and REGN7941 bound to different hIgG variants with the weakest affinities (K_D values ranged from 56 pM–3.7 nM, 76 pM–3.8 nM, and 51 pM–4.04 nM, respectively). However, the $t_{½}$ values for these AHC mAbs (ranging from 9–116 min, 10–228 min, and 9–174 min, respectively) were comparable to the spread of the $t_{½}$ values observed for the goat AHC pAb-3 (Fig. 4D); suggesting that the stability of the complexes formed between hIgG and REGN2681, REGN7779 or REGN7941 are similar to the stability of the complexes formed between hIgG and the highest

Table 3
Results of the capture kinetic analyses performed on different AHC antibodies for binding to convential hIgGs or selective hIgG variants.

			Goat AHC pAb-1				Goat AHC pAb-2				Goat AHC pAb-3				REGN2567				REGN2681				REGN7779				REGN7941				REGN7942				REGN7943			
mAb #	**hIgG Subclass**	**Details of hIgG Variants**	k_a ($M^{-1}s^{-1}$)	k_d (s^{-1})	K_D (pM)	$t_{½}$ (min)	k_a ($M^{-1}s^{-1}$)	k_d (s^{-1})	K_D (pM)	$t_{½}$ (min)	k_a ($M^{-1}s^{-1}$)	k_d (s^{-1})	K_D (pM)	$t_{½}$ (min)	k_a ($M^{-1}s^{-1}$)	k_d (s^{-1})	K_D (pM)	$t_{½}$ (min)	k_a ($M^{-1}s^{-1}$)	k_d (s^{-1})	K_D (pM)	$t_{½}$ (min)	k_a ($M^{-1}s^{-1}$)	k_d (s^{-1})	K_D (pM)	$t_{½}$ (min)	k_a ($M^{-1}s^{-1}$)	k_d (s^{-1})	K_D (pM)	$t_{½}$ (min)	k_a ($M^{-1}s^{-1}$)	k_d (s^{-1})	K_D (pM)	$t_{½}$ (min)	k_a ($M^{-1}s^{-1}$)	k_d (s^{-1})	K_D (pM)	$t_{½}$ (min)
–	hIgG1	wild-type	10.58	3.27	309	35.3	9.69	3.34	345	34.5	9.08	1.23	135	94.1	6.33	1.01	159	114.2	5.54	1.49	268.9	77.7	2.91	1.37	471	84.6	3.94	1.34	340	86.4	5.55	0.49	88.3	236.8	5.11	0.71	139	162.2
mAb-1		H435R, Y436F	10.37	2.47	238	46.8	9.65	3.27	339	35.4	9.29	1.41	152	82.0	6.75	1.17	173	98.9	5.53	1.96	354	59.0	2.90	1.77	611	65.1	4.98	1.99	400	58.0	4.84	0.76	157	152.6	4.92	0.90	183	128.2
mAb-2		Knob: T366W & Hole: T366S, L368A, Y407V, H435R, Y436F	12.36	1.70	138	67.9	11.81	2.22	188	52.1	10.84	0.69	63.3	168.5	7.51	0.98	130	118.4	4.66	2.67	571	43.3	3.36	1.47	438	78.7	3.97	1.96	494	59.0	5.83	0.48	82.9	239.2	5.28	0.59	112	194.9
mAb-6		H433K, N434F	9.05	3.14	347	36.8	8.67	3.42	395	33.8	8.21	1.49	182	77.3	4.87	1.17	240	98.8	3.36	1.60	477	72.0	2.86	1.36	475	85.1	3.14	1.46	464	79.0	3.90	0.78	200	147.2	3.04	0.81	266	142.7
mAb-10		M252Y, S254T, T256E	6.89	3.39	492	34.0	7.55	5.53	732	20.9	6.11	1.57	256	73.8	6.44	1.39	216	82.9	3.36	5.29	1570	21.9	2.64	9.54	3620	12.1	3.02	5.35	1770	21.6	5.02	1.60	318	72.3	2.96	2.24	757	51.6
mAb-11		M252Y, V308P, N434Y	9.92	4.98	502	23.2	9.48	3.73	393	30.9	8.93	1.65	185	70.1	5.85	5.62	960	20.5	3.34	12.35	3700	9.4	1.92	4.59	2400	25.2	3.17	12.80	4040	9.0	2.63	2.25	855	51.4	2.72	2.92	1070	39.6
–	hIgG2	wild-type	9.52	2.50	262	46.3	8.84	4.85	549	23.8	7.27	2.35	322	49.3	6.87	1.48	216	78.0	5.67	2.31	408	50.1	2.86	2.43	850	47.6	3.69	1.37	371	84.2	5.40	0.72	134	159.7	4.86	0.75	154	155.0
–	hIgG4	wild-type	9.08	3.87	426	29.8	8.48	8.93	1050	12.9	7.67	2.32	302	49.9	6.93	1.09	157	106.3	5.63	1.57	279	73.7	2.59	1.50	578	76.9	3.68	1.20	326	96.3	5.38	0.56	104	207.3	5.07	0.56	110	206.5
mAb-29		S228P	9.65	3.61	374	32.0	9.15	8.61	941	13.4	8.25	2.30	278	50.3	6.17	1.17	189.2	98.9	4.05	1.71	422.1	67.7	2.42	1.44	595.2	79.9	6.15	1.04	169.1	111.5	4.84	0.52	108	220.3	3.09	0.46	148.7	252.2
mAb-31		S228P, E233P, F234V, L235A, del (G236)	9.92	3.52	355	32.8	9.17	8.31	906	13.9	8.43	2.11	250	54.9	6.99	1.30	186	88.7	5.58	1.76	315	65.8	4.12	1.91	462	60.6	4.89	1.17	240	98.6	5.57	0.61	110	188.4	5.30	0.58	109	200.5

Values reported in the table are k_a (x 10^5 $M^{-1}s^{-1}$), and k_d (x 10^{-4} s^{-1}).

Table 4
List of the 43 different hIgG variants with substitutions and/or mutations in the hinge and/or Fc region characterized in the study.

IgG Variant #	hIgG Subclass	Details of hIgG Variants	Variant Abbr.	Function	Reference
mAb-1	hIgG1	H435R, Y436F	Fc*	Star substitution that abrogates Protein A binding to generate bsAbs	[12]
mAb-2		Knob: T366W & Hole: T366S, L368A, Y407V, H435R, Y436F	KIH + Fc*	Knobs-into-holes mutations to generate bsAbs and star substitution that abrogates Protein A binding	[12,13]
mAb-3		S254A, Y436A	AA	Reduced FcRn binding affinity	[14,15]
mAb-4		H310D		Reduced FcRn binding affinity	[14]
mAb-5		I253D		Reduced FcRn binding affinity and abolished binding to z-domain of Protein A	[14]
mAb-6		H433K, N434F	HN	Increased FcRn binding affinity resulting in extended PK	[16]
mAb-7		M252Y, N434Y	YY	Increased FcRn binding affinity resulting in extended PK	[17]
mAb-8		M252Y, N286E, N434Y	YEY	Increased FcRn binding affinity resulting in extended PK	[17]
mAb-9		M428L, N434S	LS	Increased FcRn binding affinity resulting in extended PK	[18]
mAb-10		M252Y, S254T, T256E	YTE	Increased FcRn binding affinity resulting in extended PK	[19]
mAb-11		M252Y, V308P, N434Y	YPY	Increased FcRn binding affinity resulting in reduced PK	[17]
mAb-12		G236A	A	Substitution for selective increase in binding affinity to FcγRIIa resulting in enhanced effector function	[36]
mAb-13		S267E, L328F	EF	Increased FcγR binding affinity resulting in enhanced effector function	[24]
mAb-14		S239D, I332E	DE	Increased FcγR binding affinity resulting in enhanced effector function	[30,31]
mAb-15		A330L		Increased FcγR binding affinity resulting in enhanced effector function	[30,31]
mAb-16		S239D, H268F, S324T, I332E	DFTE	Increased FcγR binding affinity resulting in enhanced effector function	[30,31, 37]
mAb-17		G236A, S239D, I332E	ADE	Increased FcγR binding affinity resulting in enhanced effector function	[30,31]
mAb-18		G236A, S239D, A330L, I332E	ADLE	Increased FcγR binding affinity resulting in enhanced effector function	[30,31]
mAb-19		G236A, S267E, H268F, S324T, I332E	AEFTE	Increased FcγR binding affinity resulting in enhanced effector function	[30,31]
mAb-20		L234A, L235A	LALA	Reduced FcγR and C1q binding resulting in reduced effector function	[23]
mAb-21		G236R, L328R	FcKO	Reduced FcγR binding affinity resulting in reduced effector function	[20,21]
mAb-22		D265A, N297A	DANA	Reduced FcγR binding affinity resulting in reduced effector function	[22]
mAb-23		E233P, L234V,		Reduced FcγR binding	[27–29, 33,38,39]

(*continued on next page*)

Table 4 (*continued*)

IgG Variant #	hIgG Subclass	Details of hIgG Variants	Variant Abbr.	Function	Reference
		L235A, del (G236), H268Q, K274Q, Y296F, A327G, A330S, P331S		affinity resulting in reduced effector function	
mAb-24		N297D	N297D	Reduced FcγR binding affinity resulting in reduced effector function	[34]
mAb-25		N297Q	N297Q	Reduced FcγR binding affinity resulting in reduced effector function	[34]
mAb-26		H433K, N434F, H435R, Y436F	Fc* + HN	Star substitution that abrogates Protein A binding to generate bsAbs and increased FcRn binding affinity resulting in extended PK	[12,16]
mAb-27		G236A, S267E, H268F, S324T, I332E, H435R, Y436F	Fc* + AEFTE	Star substitution that abrogates Protein A binding to generate bsAbs and increased FcγR binding affinity resulting in enhanced effector function	[12,30, 31]
mAb-28		No fucosylation			[32,35]
mAb-29	hIgG4	S228P	$IgG4^{P}$	Stabilizes the disulfides in the core-hinge of the hIgG4 and prevents Fab arm exchange	[25,26]
mAb-30		S228P, H435R, Y436F, L445P	$IgG4^{P}$ + Fc*	Star substitution that abrogates Protein A binding to generate bsAbs	[12,25, 26]
mAb-31		S228P, S267E, L328F	$IgG4^{P}$ + EF	Increased FcγR binding affinity and increased FcγR binding affinity resulting in enhanced effector function	[24–26]
mAb-32		S228P, E233P, F234V, L235A, del (G236)	$IgG4^{P}$ + PVA ($IgG4^{P-PVA}$)	Reduced FcγR binding affinity resulting in reduced effector function	[25–28]
mAb-33		S228P, E233G, F234G, del (L235)	$IgG4^{P}$ + GG ($IgG4^{P-GG}$)	Reduced FcγR binding affinity resulting in reduced effector function	[25–28]
mAb-34		S228P, E233P, F234V, L235A, del (G236), H435R, Y436F, L445P	$IgG4^{P-PVA}$ + Fc*	Reduced FcγR binding affinity resulting in reduced effector function	[12, 25–28]
mAb-35		E233P, F234V, L235A, del (G236)	$IgG4^{PVA}$	Reduced FcγR binding affinity resulting in reduced effector function	[27,28]
mAb-36		S228P, E233P, F234V, L235A, del (G236), N297Q	$IgG4^{P-PVA}$ + N297Q	Reduced FcγR binding affinity resulting in reduced effector function	[25–28, 34]
mAb-37		S228P, E233G, F234G, del (L235) N297Q	$IgG4^{P-GG}$ + N297Q	Reduced FcγR binding affinity resulting in reduced effector function	[25–28, 34]
mAb-38		S228P, M428L, N434S	$IgG4^{P}$ + LS	Increased FcRn binding affinity resulting in reduced PK	[18,25, 26]
mAb-39		S228P, M252Y, S254T, T256E	$IgG4^{P}$ + YTE	Increased FcRn binding affinity resulting in reduced PK	[19,25, 26]
mAb-40		S228P, H433K, N434F	$IgG4^{P}$ + HN	Increased FcRn binding affinity resulting in reduced PK	[16,25, 26]
mAb-41		S228P, M252Y, N286E, N434Y	$IgG4^{P}$ + YEY	Increased FcRn binding affinity resulting in reduced PK	[17,25, 26]
mAb-42		S228P, H433K, N434F, H435R, Y436F, L445P	$IgG4^{P}$ + Fc* + HN	Star substitution that abrogates Protein A binding to generate	[12,16, 25,26]

(*continued on next page*)

Table 4 (*continued*)

IgG Variant #	hIgG Subclass	Details of hIgG Variants	Variant Abbr.	Function	Reference
				bispecific antibody and increased FcRn binding affinity for extended PK	
mAb-43		S228P, E233G, F234G, del (L235), M252Y, S254T, T256E	$IgG4^{P-GG}$ + YTE	Reduced FcγR binding affinity resulting in reduced effector function and increased FcRn binding affinity resulting in extended PK	[19, 25–28]

affinity goat AHC pAb (pAb-3). REGN2567 bound to different hIgG variants with K_D values ranging from 36–960 pM (comparable to the goat AHC pAb-3), but exhibited longer $t_{½}$ values (ranging from 21–199 min), indicating that REGN2567-hIgG complexes are more stable than the hIgG complexed with the goat AHC pAb-3. Both REGN7942 and REGN7943, which bound to canonical hIgG1, hIgG2, and hIgG4 with the highest affinity and longest $t_{½}$ (Table 3) continued to show the highest affinity binding to the 43 different hIgG variants; K_D values ranged from 7.77–855 pM and 18.1 pM – 1.07 nM and $t_{½}$ values ranging from 51–913 min and 40–442 min, respectively. Of the 43 hIgG variants tested, mAb-11 (M252Y, V308P, N434Y) had the broadest impact on binding to mouse AHC mAbs (Supplementary Table 3). However, REGN7942 and REGN7943 still retained their high affinity binding to mAb-11 with K_D values of 855 pM and 1.07 nM and $t_{½}$ values of 51 and 40 min, respectively, stronger than the binding affinity of wild-type hIgG to goat AHC pAb-1 and pAb-2.

3.4. Mouse AHC mAb surfaces captured high levels of hmAbs and retained its binding activity following extensive capture-regeneration cycles

Evaluation of the six mouse AHC mAbs for use as hmAb capture reagents was further assessed by examining the three critical properites of a good capture reagent: (i) retention of high binding activity following covalent immobilization onto the sensor surface, (ii) ability to capture high levels of mAb even at low concentrations, and (iii) capable of withstanding multiple capture-regeneration cycles without substantial loss in the binding activity. Prior to immobilization, it was empirically determined that 10 mM sodium acetate, pH 5.0 was best suited for pre-concentration of all six mouse AHC mAbs into the dextran matrix of the Biacore sensor chip. The AHC mAbs were immobilized onto different CM5 sensor surfaces using the standard EDC/NHS chemistry and a 10 min injection of 20 μg/mL mouse AHC mAb achieved immobilization levels of approximately 10,000–12,000 RU. Before testing the binding activity of different AHC mAb immobilized surfaces, a regeneration condition was established for complete removal of captured hmAbs without affecting the surface activity. A wide range of regeneration conditions were evaluated by screening various regeneration buffers and injection times, and a single 4 s injection of 20 mM phosphoric acid was found to be optimal to regenerate all six mouse AHC mAb surfaces. Having optimized the regeneration conditions, fresh CM5 sensor surfaces were derivatized with different mouse AHC mAbs and their binding activity was assessed. The three goat AHC pAbs were also immobilized onto the sensor surface and used as benchmark surfaces to compare the binding activity of the six mouse AHC mAbs.

The binding capacity of different AHC immobilized sensor surfaces was assessed by injecting varying concentrations of hIgG1, hIgG2, hIgG4 or $hIgG4^P$ (0.1, 0.5, 2, 10 μg/mL) for 3 min and the stability of the captured hIgGs was monitored for 10 min. Fig. 5 shows the real-time binding sensorgrams of different hIgG subclasses binding to AHC surfaces, and the observed capture levels are reported in Table 5. All three goat AHC pAb surfaces exhibited similar hIgG capture profiles; highest binding response was observed for hIgG1 followed by hIgG2, hIgG4 and $hIgG4^P$. Injection of 10 μg/mL hIgG1 almost saturated the surface at ~1300–1500 RU, while binding responses of ~836–966 RU was observed for $hIgG4^P$. The shape of the binding sensorgrams for 2 μg/mL hIgG injection were non-linear, while linear binding curves were observed for 0.5 μg/mL and 0.1 μg/mL hIgG concentrations (Supplementary Fig. 1).

In contrast, more than 2.5-fold higher binding responses were detected for all six mouse AHC mAb surfaces at 10 μg/mL of hIgG. REGN2567 and REGN2681 surfaces showed the highest binding activity (~3800–4600 RU), while the REGN7943 surface had the lowest binding activity (~3200–3800 RU). The remaining three mouse AHC mAb surfaces (REGN7779, REGN7941 and REGN7942) demonstrated similar binding activity. Between different hIgG subclasses, highest binding was observed for hIgG1 followed by hIgG2, hIgG4 and $hIgG4^P$; similar to the goat AHC pAb surfaces. The hIgG binding sensorgrams were mostly linear, even at 10 μg/mL, suggesting that all six mouse AHC mAb surfaces have the capacity to capture more than 4500 RU of hIgG. It was intriguing that even at such high capture levels all captured hIgGs were very stable, with no noticeable drop in the binding response during the 10 min dissociation phase. The hIgG binding to all six mouse AHC mAb surfaces at 2 μg/mL were similar to 10 μg/mL hIgG captured on the three goat AHC pAb surfaces. However, unlike the saturation observed for the goat AHC pAb surfaces at 10 μg/mL hIgG (~1300–1500 RU); the shape of the sensorgrams for 2 μg/mL hIgG binding to different mouse AHC mAb surfaces was linear; suggesting that higher binding can be achieved with extended injection times. At 0.5 μg/mL hIgG; ~1.5-2-fold higher binding was detected for all six mouse AHC mAb surfaces, while at 0.1 μg/mL hIgG the three goat AHC pAb and six mouse AHC mAb surfaces showed comparable binding responses. These data show that all six mouse AHC mAb surfaces presented in this study have much higher hIgG binding capacity compared to the goat AHC pAb surfaces and exhibit sensitivity similar to the three goat AHC pAb surfaces at 0.1 μg/mL hIgG concentration. Such binding properties will not only allow capturing high density hIgG; required for the characterization of small Ags with molecular weights less than 1 kD but will also enable the kinetic screening of unpurifed mAb in CM with low expression levels.

The ability for AHC mAbs to reproducibly capture different hIgG subclasses following multiple capture-regeneration cycles was next examined. Our group routinely performs capture kinetic assays at 25°C and at physiological temperature (37°C) and we typically observe loss in the binding activity of all three goat AHC pAb surfaces at 37°C, but not at 25°C. We understand that surface regeneration performed at higher temperatures is typically more abrasive and hence we opted to assess hIgG capture reproducibility at 37°C. For a typical capture kinetic assay, we aim to achieve 30–100 RU of maximum binding response (Rmax) by capturing 50 RU to 600 RU of hmAbs binding to Ag with molecular weights ranging from 150kD to 5kD, respectively. Therefore, a density of ~600–650 RU was selected to assess capture reproducibility of different mouse AHC mAb surfaces. Moreover, to add rigor in our assessment of AHC mAb surfaces, we decided to examine hIgG capture reproducibility for over 300 capture-regeneration cycles. Fig. 6 shows the bar graph of the average capture levels of hIgG1, hIgG2, hIgG4 or $hIgG4^P$ from over 300 capture-regeneration cycles while their respective real time binding sensorgrams are provided in Supplementary Fig. 2. No change in the binding activity was observed for any mouse AHC mAb surfaces even after 300 surface regenerations at 37°C.

Based on the data presented, all six mouse AHC mAbs reported in this study showed very similar binding profiles and exhibit properties superior to the three goat AHC pAbs – (i) specifically bind to the Fc region

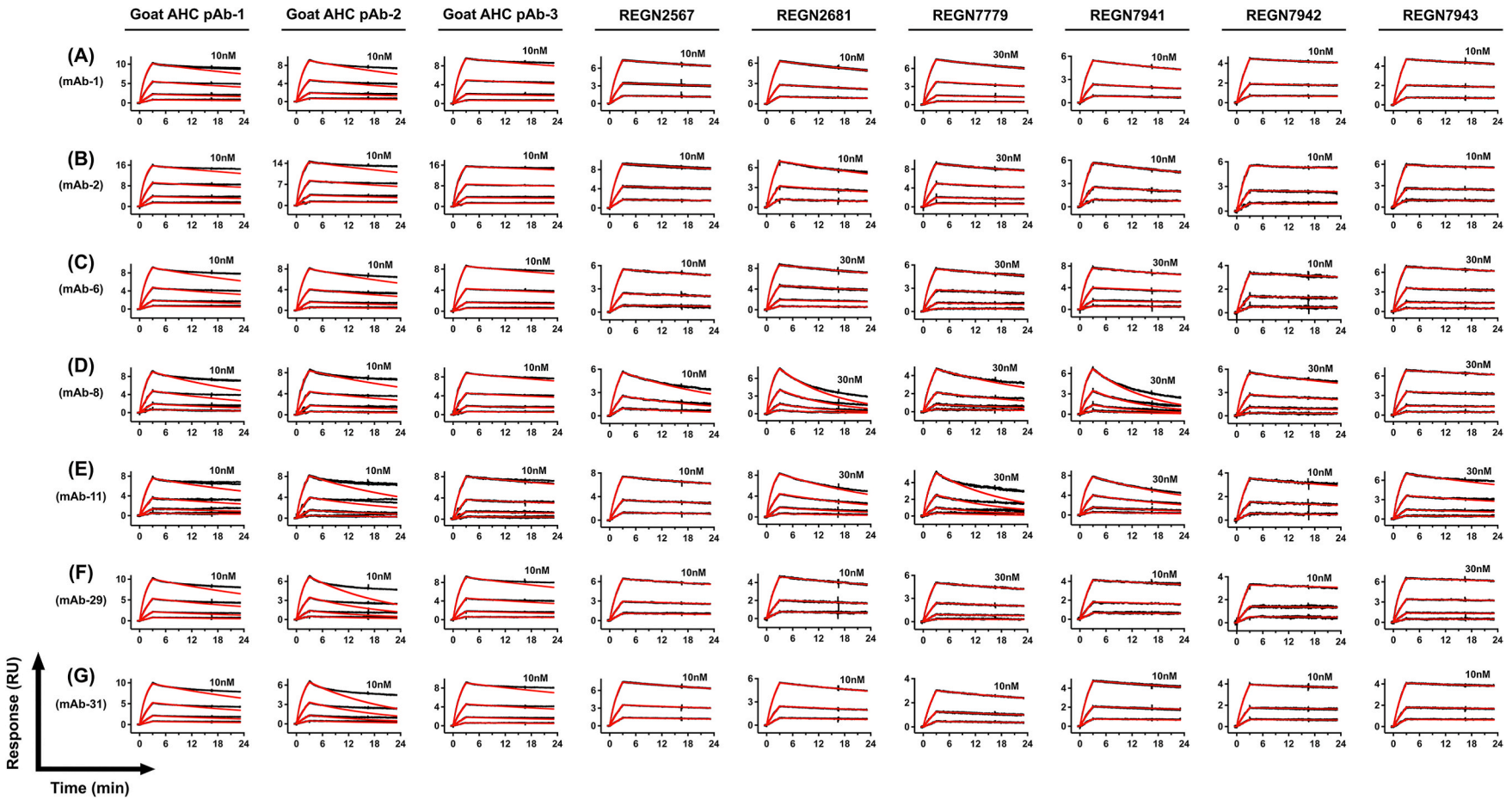

Fig. 3. Binding of different AHC antibodies to six representative hmAb variants. Different goat AHC pAbs or mouse AHC mAbs were captured at a very low density (3–7 RU) using mouse anti-goat Fc mAb or rabbit anti-mouse Fc pAb surfaces, respectively. Different concentrations of hIgG variants (serially diluted by three-fold) were later injected for 3 min followed by a 20 min dissociation time. Sensorgrams for seven of the 43 hIgG variants listed in Table 4 are shown: (**A**) mAb-1, (**B**) mAb-2, (**C**) mAb-6, (**D**) mAb-10, (**E**) mAb-11, (**F**) mAb-29, or (**G**) mAb-31. The mAbs are either expressed as a hIgG1 (A–E) or as a hIgG4 (F–G). The real time binding sensorgrams (shown in black) represent duplicate injections of each hIgG concentration, while the fits generated by globally fitting the binding sensorgrams using 1:1 binding model with mass transport limitation is shown as red lines. The highest hIgG concentration used to fit the data is provided and the results of the kinetic analyses are listed in Table 3. (For interpretation of the references to color in this figure legend, the reader is referred to the Web version of this article.)

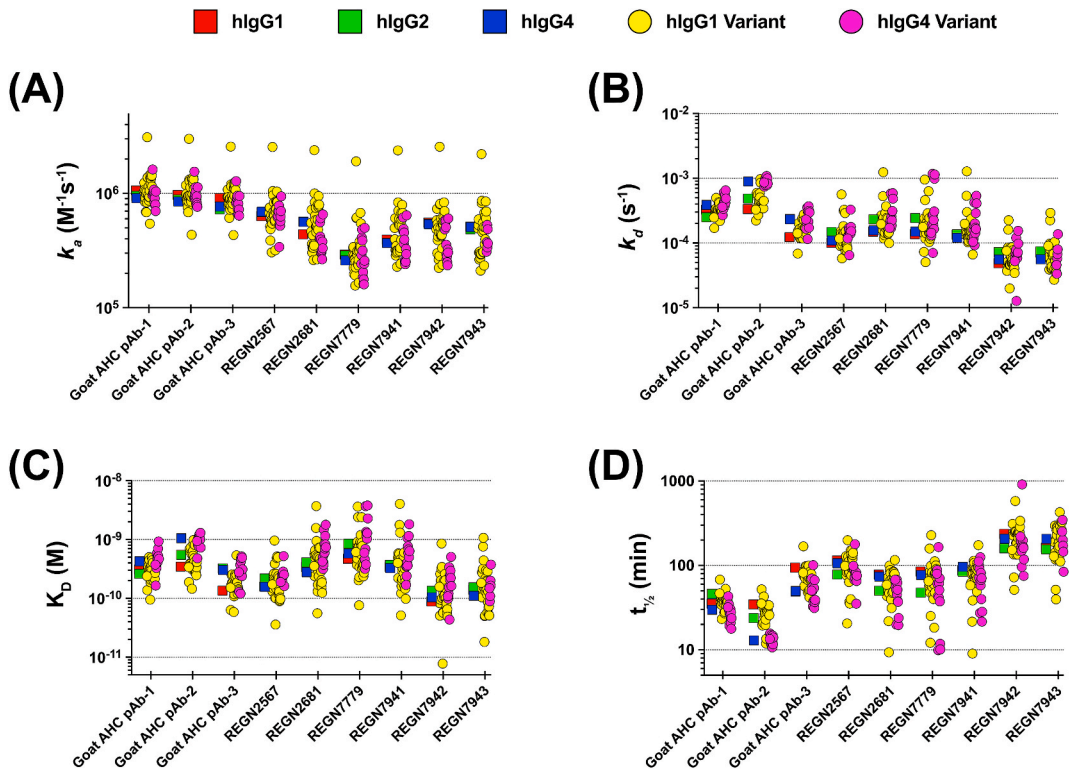

Fig. 4. Comparison of binding kinetic data performed on six mouse AHC mAbs and three goat AHC pAbs for binding to three wild-type hIgG and 43 different hIgG variants. The scatter plot shows (**A**) k_a, (**B**) k_d, (**C**) K_D, (**D**) $t_{½}$ values of different AHC antibodies binding to wild-type hIgG1 (■), hIgG2 (■), hIgG4 (■), or different variants of hIgG1 (●) or hIgG4 (●).

of a diverse set of hIgG variants with high affinity, (ii) sensor surfaces immobilized with AHC mAb show higher hIgG binding capacity and binding sensitivity to capture hIgG at 0.1 μg/mL concentration, (iii) reproducibly capture ~600–650 RU of hIgG even after 300 capture-regeneration cycles at 37°C. However, among all six mouse AHC mAbs, REGN7942 and REGN7943 showed the best overall binding to different hIgG variants; sub-nanomolar affinity with slow dissociation rates ($t_{½}$ values ranging from 51–913 min and 40–442 min, respectively) (Supplementary Table 3) and we therefore selected REGN7942 and REGN7943 for further evaluation as capture reagents.

It has been reported that the negatively charged carboxyl groups in the dextran matrix of a CM5 sensor chip can adversely affect the results of kinetic assays performed on an optical biosensor and it is recommended to perform binding kinetic studies on CM4 and C1 sensor chips which have fewer carboxyl groups [40]. In comparison to a CM5 sensor chip, the dextran surface of a CM4 sensor chip contains approximately 70% fewer carboxyl groups; while the planar C1 sensor chip lacks the dextran layer and contains 90% fewer carboxyl groups [40]. Proteins are typically immobilized onto the carboxyl group of a Biacore chip and as a result the protein immobilization levels are typically proportional to the number of carboxyl groups (CM5 > CM4 > C1). Therefore, in order to allow the characterization of mAb binding over a wide range of Ag molecular weights (>5 kD), a high hIgG binding capacity for the AHC antibody immobilized surface would be preferred, especially for the C1 sensor chip.

Binding studies similar to Fig. 5 were performed on CM4 and C1 sensor chips by individually immobilizing REGN7942, REGN7943 or each of the three goat AHC pAbs on different sensor surfaces. The standard EDC/NHS surface chemistry was performed and a 10 min injection of 25 μg/mL of AHC antibodies yielded immobilization levels of approximately 4000–5000 RU and 1000 RU on a CM4 and C1 sensor chips, respectively. Varying concentrations of hIgG1, hIgG2, hIgG4 or $hIgG4^P$ (0.1, 0.5, 2, 10 μg/mL) were injected for 3 min with a 10 min dissociation phase and the average binding responses of four separate injections are shown in Fig. 7, while their respective binding responses (± standard deviation) are provided in Supplementary Table 4. Similar to the CM5 sensor chip, both REGN7942 and REGN7943 surfaces exhibited the highest hIgG binding capacity and approximately 2500–3500 RU and 750–800 RU of hIgG bound to CM4 and C1 sensor surfaces, respectively. The goat AHC pAb-2 surface continued to exhibit the lowest hIgG binding response with a capacity of around 270–560 RU and 130–190 RU on a CM4 and C1 sensor surface, respectively. Both goat AHC pAb-1 and goat AHC pAb-3 surfaces showed similar binding capacity and binding responses of 500–1000 RU and 170–350 RU were observed on CM4 and C1 sensor surfaces, respectively. All hIgGs bound to the three goat AHC pAb immobilized CM4 surfaces with excellent baseline stability and no dissociation from any surfaces was observed during the 10 min dissociation phase (Supplementary Fig. 3). Conversely, the same three goat AHC pAbs once immobilized on the C1 sensor surface displayed noticeable hIgG dissociation, particularly at 2 μg/mL and 10 μg/mL hIgG concentrations (Fig. 8). Between the different hIgGs included in the study, hIgG1 was the most stable captured surface followed by hIgG2, while the dissociation of hIgG4 and $hIgG4^P$ were comparable. The hIgG dissociation rate at 0.5 μg/mL seemed to be slower than 2 μg/mL and 10 μg/mL concentrations while the hIgG binding at 0.1 μg/mL concentration was most stable. Such binding profiles would limit the utility of the goat AHC pAb surfaces to capture at most 80 RU of mAb which could be a challenge to characterize mAb binding to a 5kD antigen (Rmax of less than 5 RU) especially for high affinity interactions exhibiting slow dissociation rate constants ($k_d < 5 \times 10^{-5}$ s^{-1}). In contrast, 750–800 RU binding levels were observed on REGN7942 and REGN7943 immobilized C1 surfaces which is almost four times the binding response observed for the goat AHC pAb surfaces. It was also encouraging to discover that even at such capture densities, all hIgGs were stably captured onto REGN7942 and REGN7943 immobilized C1 surfaces with no drop in the binding response during the 10

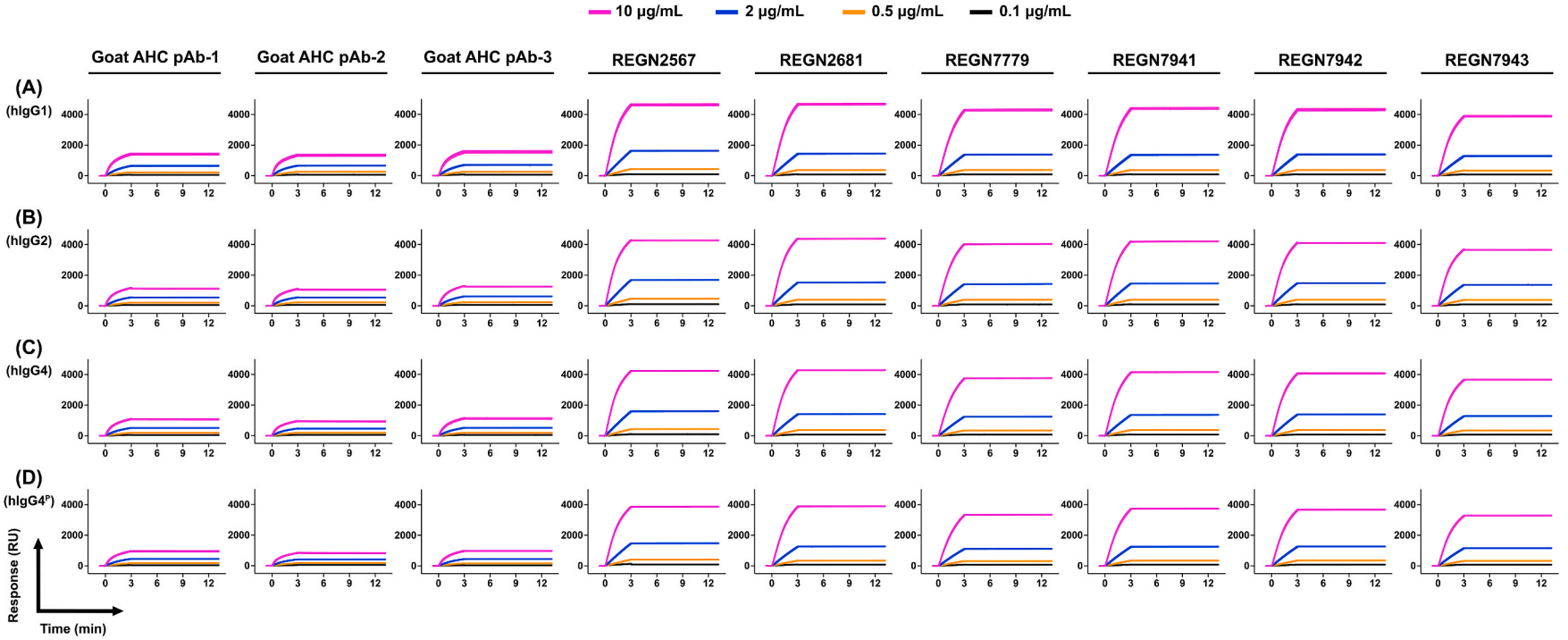

Fig. 5. Binding capacity of different AHC capture antibody surfaces on a CM5 sensor chip. Approximately 10,000–12,000 RU of different AHC antibodies were individually immobilized on different surfaces of a CM5 sensor chip. Varying concentrations of (**A**) hIgG1, (**B**) hIgG2, (**C**) hIgG4, or (**D**) hIgG4^{P} were injected for 3 min followed by a 10 min dissociation phase. Binding sensorgrams are color coded based on the injected hIgG concentrations and an overlay of four replicate injections for each hIgG concentration is shown. (For interpretation of the references to color in this figure legend, the reader is referred to the Web version of this article.)

Table 5
Binding of varying concentrations of hIgG1, hIgG2, hIgG4 or hIgG4^P to different AHC antibody immobilized surfaces. The hIgG binding levels reported in the table are the average of four separate injections ± standard deviation.

	hIgG1 Binding (RU)				hIgG2 Binding (RU)				hIgG4 Binding (RU)				hIgG4P Binding (RU)			
AHC Surface	**0.1 µg/mL**	**0.5 µg/mL**	**2 µg/mL**	**10 µg/mL**	**0.1 µg/mL**	**0.5 µg/mL**	**2 µg/mL**	**10 µg/mL**	**0.1 µg/mL**	**0.5 µg/mL**	**2 µg/mL**	**10 µg/mL**	**0.1 µg/mL**	**0.5 µg/mL**	**2 µg/mL**	**10 µg/mL**
Goat AHC pAb-1	64 ± 0.6	225 ± 1.3	637 ± 8.1	1388 ± 38.9	63 ± 0.3	209 ± 0.5	550 ± 2.5	1157 ± 12.3	53 ± 0.2	193 ± 1.2	504 ± 3.7	1079 ± 17.5	50 ± 0.3	174 ± 0.4	448 ± 2.3	944 ± 14.1
Goat AHC pAb-2	71 ± 0.7	246 ± 1.6	685 ± 10.6	1518 ± 55.0	70 ± 0.3	233 ± 0.5	606 ± 2.0	1284 ± 8.1	53 ± 0.2	190 ± 1.3	504 ± 4.3	1118 ± 23.9	49 ± 0.3	169 ± 0.4	441 ± 2.4	966 ± 16.3
Goat AHC pAb-3	71 ± 0.5	254 ± 2.1	647 ± 7.9	1316 ± 40.9	66 ± 0.8	223 ± 1.0	531 ± 3.2	1045 ± 14.0	57 ± 0.1	196 ± 0.8	468 ± 2.0	942 ± 12.6	56 ± 0.4	180 ± 0.9	420 ± 2.2	836 ± 8.5
REGN2567	94 ± 0.2	413 ± 2.0	1572 ± 7.5	4571 ± 41.7	100 ± 0.1	443 ± 0.2	1627 ± 1.5	4200 ± 8.2	96 ± 0.9	418 ± 1.6	1546 ± 5.9	4176 ± 6.2	96 ± 0.2	392 ± 1.8	1420 ± 2.9	3805 ± 5.3
REGN2681	79 ± 0.3	352 ± 1.9	1383 ± 11.3	4586 ± 35.5	85 ± 0.1	382 ± 0.3	1462 ± 1.9	4296 ± 7.9	78 ± 0.4	355 ± 0.9	1359 ± 2.6	4210 ± 4.8	78 ± 0.5	327 ± 2.1	1218 ± 6.9	3807 ± 7.3
REGN7779	81 ± 0.2	356 ± 1.4	1322 ± 9.3	4204 ± 32.9	86 ± 0.1	380 ± 0.2	1360 ± 1.1	3935 ± 7.1	75 ± 0.4	335 ± 0.5	1206 ± 1.3	3675 ± 3.3	73 ± 0.5	305 ± 1.8	1073 ± 5.6	3262 ± 6.5
REGN7941	77 ± 0.1	344 ± 1.1	1296 ± 14.7	4299 ± 37.4	85 ± 0.2	376 ± 0.2	1393 ± 0.7	4102 ± 6.0	77 ± 0.3	353 ± 1.8	1312 ± 1.8	4061 ± 7.8	76 ± 0.4	328 ± 2.4	1202 ± 7.8	3657 ± 10.6
REGN7942	79 ± 0.1	355 ± 1.1	1341 ± 19.6	4250 ± 45.4	87 ± 0.1	388 ± 0.2	1430 ± 0.9	4031 ± 9.1	79 ± 0.2	364 ± 1.5	1347 ± 3.1	4003 ± 11.1	80 ± 0.3	338 ± 3.1	1223 ± 7.9	3601 ± 12.0
REGN7943	73 ± 0.1	329 ± 2.0	1243 ± 15.5	3820 ± 26.3	80 ± 0.2	361 ± 0.7	1320 ± 1.0	3588 ± 5.9	72 ± 0.1	337 ± 0.7	1239 ± 4.6	3592 ± 9.8	74 ± 0.3	312 ± 2.5	1115 ± 9.7	3223 ± 6.9

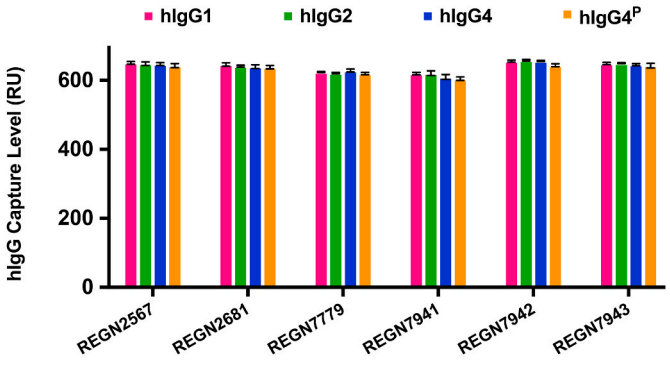

Fig. 6. Reproducibility of hIgG captured on six mouse AHC mAb surfaces following multiple capture-regeneration cycles. 600–650 RU of hIgG1, hIgG2, hIgG4 or hIgG4^P was captured on a CM5 sensor chip individually immobilized with six different mouse AHC mAbs at 37°C followed by surface regeneration using a 4 s injection of 20 mM phosphoric acid. The reproducibility of hIgG capture levels was assessed by running more than 300 capture-regeneration cycles and the average capture level is plotted (±standard deviation).

min dissociation phase (Fig. 8).

Based on these exciting binding capacity data, we expanded the scope of the current study and investigated the long term capture stability of the REGN7942 and REGN7943 immobilized surfaces. The CM5, CM4 and C1 sensor surfaces were individually immobilized with REGN7942 and REGN7943 and the results of long term capture stability were compared with the three goat AHC pAb surfaces. Since similar profiles were observed for REGN7942 and REGN7943 binding to different hIgG subclasses and the in-house antibodies are typically expressed as either hIgG1 or hIgG4^P, we opted to only include hIgG1 and hIgG4^P in the long term capture stability study. We were only able to test capture stability for 10,000 s (2 h and 47 min), as it is the longest allowable dissociation time for the "analyte" injection command on the Biacore 8k biosensor. Around 400–500 RU of hIgG1 or hIgG4^P were captured on CM5 and CM4 immobilized surfaces but only 150–200 RU density of hIgG was captured on C1 chip due to the significantly reduced binding capacity for the goat AHC pAb surfaces. Unfortunately, since the hIgG binding capacity for the goat AHC pAb-2 immobilized C1 surface was much lower than the other two goat AHC pAbs, the long term stability for the goat AHC pAb-2 immobilized C1 surface was tested only at approximately 100 RU hIgG capture level. The hIgG1 or hIgG4^P concentrations were empirically determined to achieve desired capture levels and an overlay of the binding sensorgrams from at least three separate injections is provided in Fig. 9. All five AHC antibody surfaces (REGN7942, REGN7943 and three goat AHC pAbs) exhibited excellent baseline stability on both CM5 and CM4 sensor chips during the 10,000 s dissociation phase. However, none of the goat AHC pAb surfaces stably captured any hIgG on the C1 sensor chip, which was not surprising especially based on the binding capacity data shown in Fig. 8. A gradual dissociation of hIgG1 was observed and approximately 20–30% of captured hIgG1 dissociated during the 10,000 s dissociation phase. The capture stability for hIgG4^P was even more inferior with an approximately 50% drop in capture level within 20 min of dissociation.

Conversely, both REGN7942 and REGN7943 immobilized C1 sensor surfaces stably captured both hIgG1 and hIgG4^P without any noticeable drop in the binding response during the 10,000 s dissociation phase. To further push the experimental limits and add rigor to our assessment, we repeated the same long term stability study by capturing 500 RU of hIgG on the REGN7942 and REGN7943 surfaces which would allow a fair comparison of the C1 stability results with those generated on the CM5 and CM4 sensor chips. Even at such high capture levels, no drop in the hIgG binding response was observed and all four replicate injections overlapped (Supplementary Fig. 4). This is an extremely important finding as 500 RU mAb capture density would typically be required to characterize binding of an Ag with a molecular weight of 5kD or less (Rmax <30 RU), which would be challenging for mAb density of less than 80 RU (Rmax <5 RU); the stable mAb capture level observed for all three goat AHC pAb surfaces.

3.5. Capture kinetic analyses performed using REGN7942 and REGN7943 surfaces are in concordance with the three goat AHC pAb surfaces

Our data showed that REGN7942 and REGN7943 had faster dissociation rates for certain Fc variants, especially mAb-11 (M252Y, V308P, N434Y) as reported in Supplementary Table 3. However, the $t_{½}$ values for binding to this Fc mutant (51 min and 40 min for REGN7942 and REGN7943, respectively) were comparable to the $t_{½}$ values measured for goat AHC pAbs binding to canoncical hIgGs. To ensure that the results of capture kinetic analyses performed using REGN7942 and REGN7943 immobilized surfaces are not affected by such variants, two hmAbs that

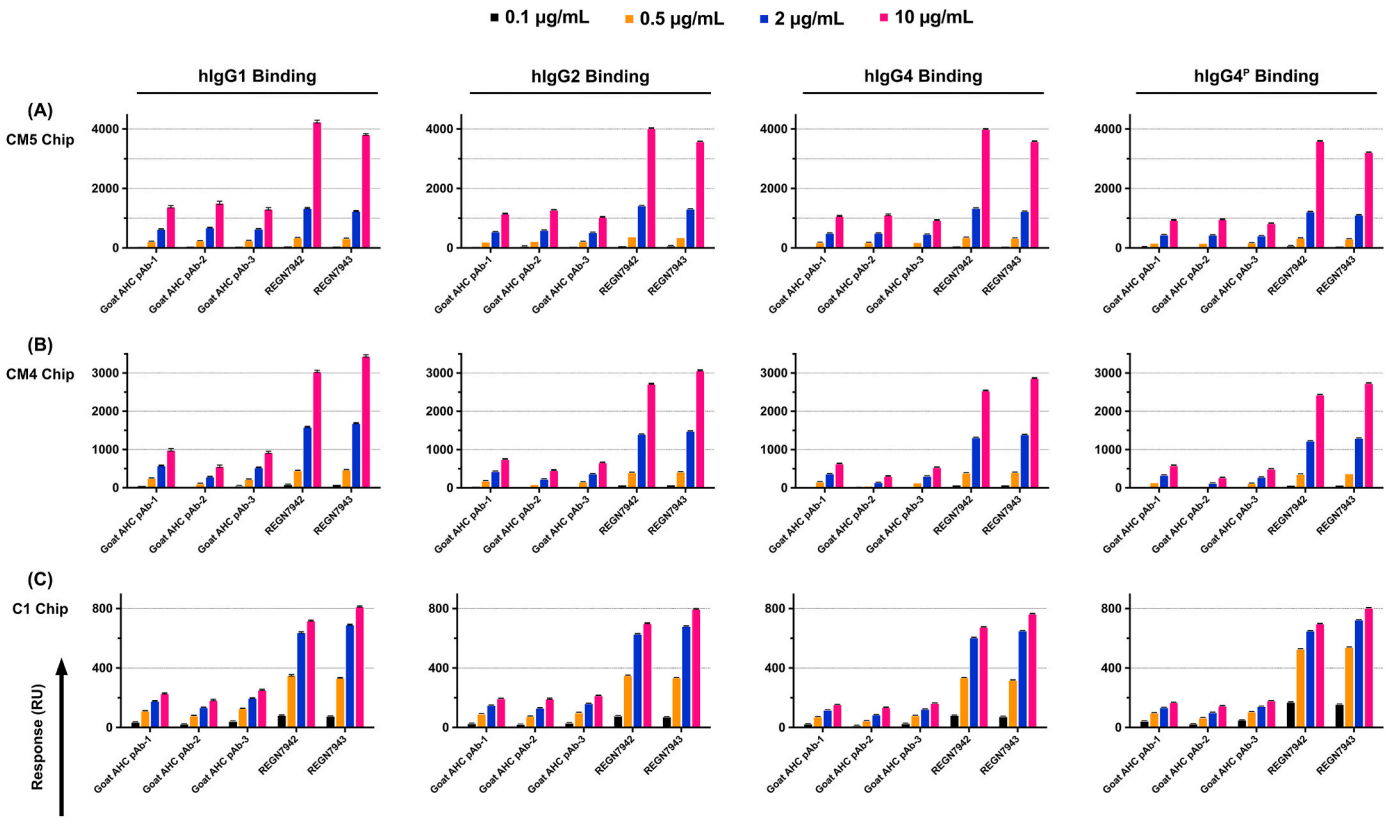

Fig. 7. Binding capacity of REGN7942, REGN7943 and the three goat AHC pAbs immobilized on CM5, CM4 and C1 sensor chips. REGN7942, REGN7943 or the three goat AHC pAbs were individually immobilized on different surfaces of CM5, CM4 and C1 sensor chips at a density of 10000–12000 RU, 4000–5000 RU and 1000 RU, respectively. Varying concentrations of hIgG1, hIgG2, hIgG4 or hIgG4^P (0.1, 0.5, 2, 10 µg/mL) were injected for 3 min with a 10 min dissociation phase. An aveage of four replicate injections for each hIgG concentration is plotted (±standard deviation).

bind discrete Ags with high affinity were expressed as multiple hIgG variants and their Ag binding kinetics were determined. The hmAb-1 through hmAb-15 bind a 21.9kD Ag (Ag-1), while hmAb-16 through hmAb-27 bind to a 74.7kD Ag (Ag-2). Both Ags are soluble targets and the details of hmAbs along with the 27 different hIgG variants (3 wild-type and 24 mutants) tested are provided in Table 6.

The kinetics of Ag-1 and Ag-2 binding to their respective hmAbs expressed as canonical hIgGs and selective hIgG variants were first characterized using the three goat AHC pAb surfaces. The binding of Ag-1 to hmAb, expressed as conventional hIgGs (hIgG1, hIgG2 and hIgG4) or hIgG4^P, and Ag-2 binding to hmAb, expressed as hIgG4^P, were included in the study. Our data showed that hIgG1 expressed with M252Y, V308P, N434Y variant profoundly impacted the binding to the six mouse AHC mAbs (a 3-10-fold faster dissociation rate), but not to any of the goat AHC pAbs (Table 3). We therefore used goat AHC pAb capture surfaces to characterize Ag-2 binding to hmAb expressed with this specific variant, so that we could account for any possible discrepancies in the measurement of the hmAb-Ag interactions. The k_a, k_d, and K_D values measured for these hmAbs using goat AHC pAb surfaces were later compared to those determined for Ag binding to hmAb expressed as 27 different hIgG variants using REGN7942 and REGN7943 capture surfaces.

Around 90 RU and 35 RU of hmAb binding to Ag-1 and Ag-2, respectively, were captured on different goat AHC pAb surfaces and varying concentrations of Ag-1 or Ag-2 (three-fold serial dilution) were injected for 3 min with a 15 min of dissociation phase. The results of the kinetic analyses are provided in Table 7 and the real time binding sensorgrams with the global fits are shown in Fig. 10. The hmAbs specific to Ag-1 or Ag-2 bound with a K_D of 0.7 nM and 1.1 nM, respectively. No significant difference in the kinetic values was observed for Ag-1 binding to hmAb expressed as hIgG1, hIgG2, hIgG4 or hIgG4^P. Similarly, binding kinetic values measured for Ag-2 binding to hmAb expressed as hIgG4^P or as hIgG1 expressed with M252Y, V308P, N434Y variant were also in concordance.

We next performed capture kinetic analyses using REGN7942 and REGN7943 surfaces using all 27 variants of hmAbs to examine their binding to their respective Ag. The results of Ag-1 or Ag-2 binding to hmAbs expressed as hIgG1, hIgG2, hIgG4, hIgG4^P and as hIgG1 expressed with M252Y, V308P, N434Y variant are provided in Table 7, while their real time binding sensorgrams are shown in Fig. 10. Supplementary Table 5 provides the results of hmAb-Ag capture kinetic assays for the entire set of 27 hmAbs, while Supplementary Fig. 5 shows their affinity isotherm plot (k_a vs k_d). The binding kinetic values generated using REGN7942 and REGN7943 surfaces were in concordance with the values measured on the goat AHC pAb surfaces. None of the hIgG variants affected the results of the kinetic analyses and less than two-fold difference in the k_a, k_d, and K_D values were observed for both Ag-1 and Ag-2.

We previously reported that the capture kinetic analyses performed on six picomolar affinity hmAbs using a commercial mouse AHC mAb surface measured up to 14-17-fold weaker binding affinities compared to goat AHC pAb surfaces [10]. Four out of the six picomolar affinity hmAbs binding to 14.8kD, 17.9kD, 27.7kD, and 57.8kD Ags that were characterized using mouse AHC mAb surfaces generated binding affinities that were more than four-fold weaker than those measured with the goat AHC pAb surfaces. To investigate whether REGN7942 and REGN7943 surfaces could reliably determine the k_a, k_d and K_D values of hmAb-Ag interactions, we repeated capture kinetic analyses on these four picomolar hmAbs using REGN7942, REGN7943 and the three goat AHC pAb surfaces. Similar levels of hmAb were captured on different AHC antibody surfaces, followed by the injection of varying concentrations of specific Ag (serially diluted by three-fold) for 3 min. As

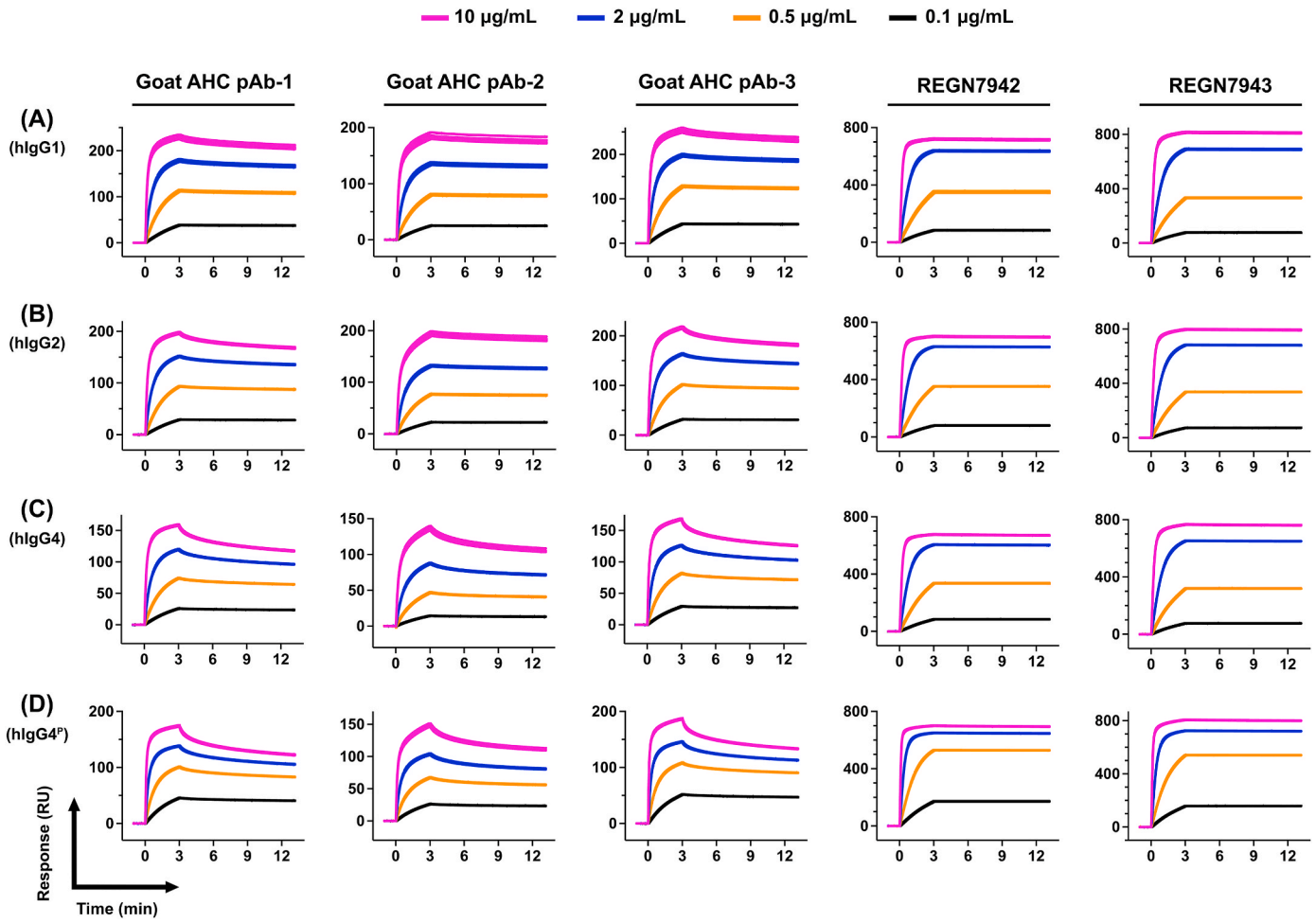

Fig. 8. Binding capacity of REGN7942, REGN7943 and the three goat AHC pAb surfaces on a C1 sensor chip. Approximately 1000 RU of REGN7942, REGN7943 or the three goat AHC pAbs were individually immobilized on different surfaces of a C1 sensor chip. Varying concentrations of (**A**) hIgG1, (**B**) hIgG2, (**C**) hIgG4, or (**D**) hIgG4^{P} were injected for 3 min followed by a 10 min dissociation phase. Binding sensorgrams are color coded based on the hIgG concentrations and an overlay of four replicate injections for each hIgG concentration is shown. (For interpretation of the references to color in this figure legend, the reader is referred to the Web version of this article.)

performed previously, Ag dissociation was monitored for 1 h to ensure that at least a 5% drop in the binding response was observed. Results of the kinetic analyses performed on the four picomolar affinity hmAb-Ag interactions are provided in Table 8 and the real time binding sensorgrams with global fits are shown in Fig. 11.

As reported previously [10], the kinetic values measured for all four picomolar affinity hmAbs were comparable between the three goat AHC pAb surfaces and the K_D values measured for hmAb binding to 14.8kD, 17.9kD, 27.7kD, and 57.8kD Ag were 33–47 pM, 113–138 pM, 44–51 pM, and 57–64 pM, respectively. The binding kinetic values determined in this study on the Biacore 8k biosensor (Table 8) were also comparable to the values determined previously using the Biacore 4000 biosensor [10], supporting that the binding kinetic assays performed on different SPR biosensors generate similar results. It was encouraging to see that hmAb-Ag interactions characterized on REGN7942 and REGN7943 surfaces yielded k_a, k_d, and K_D values within two-fold of the values measured using the three goat AHC pAb surfaces. Collectively, our results show that both REGN7942 and REGN7943 are ideal AHC capture reagents exhibiting properties superior to the three goat AHC pAbs included in this study and the results of the capture kinetic analyses performed on the label-free biosensor using these capture surfaces are in concordance with the data generated using the three goat AHC pAb surfaces.

4. Discussion

We previously reported that the commonly used commercial reagents for performing capture kinetic analyses on a label-free optical biosensor, such as Protein A, Protein G, Protein A/G, Protein L and a mouse AHC mAb can generate unreliable k_a, k_d, and K_D values of hmAb-Ag interactions [10]. Instead, high affinity, Fc specific antibodies, such as the three goat AHC pAbs, are the preferred reagents to generate reliable binding kinetic values. Although all three goat AHC pAbs provide reasonable options for capturing hmAbs, they present several challenges. Surfaces immobilized with any of the three goat AHC pAbs exhibit a low binding capacity and at least a 3 min injection of 2 µg/mL of hIgG is required to achieve capture levels of approximately 600 RU on a CM5 chip. The hIgG binding capacity is also significantly reduced on a C1 sensor chip and a 3 min injection of 10 µg/mL hIgG only yielded 170–350 RU of binding response (Fig. 7). Moreover, the observed poor hIgG capture stability, especially for IgG4^{P} which showed an almost 50% drop in capture levels during the first 20 min of dissociation phase, make these goat AHC pAbs less favorable as capture reagents for performing capture kinetic analyses on a C1 sensor chip (Fig. 9). These binding profiles can potentially limit the utility of these surfaces to perform high throughput capture kinetic screening of (i) mAbs in CM for low expressing clones and/or (ii) mAbs that bind Ags with molecular weight less than 5kD and/or (iii) mAbs binding to Ag using a C1 sensor

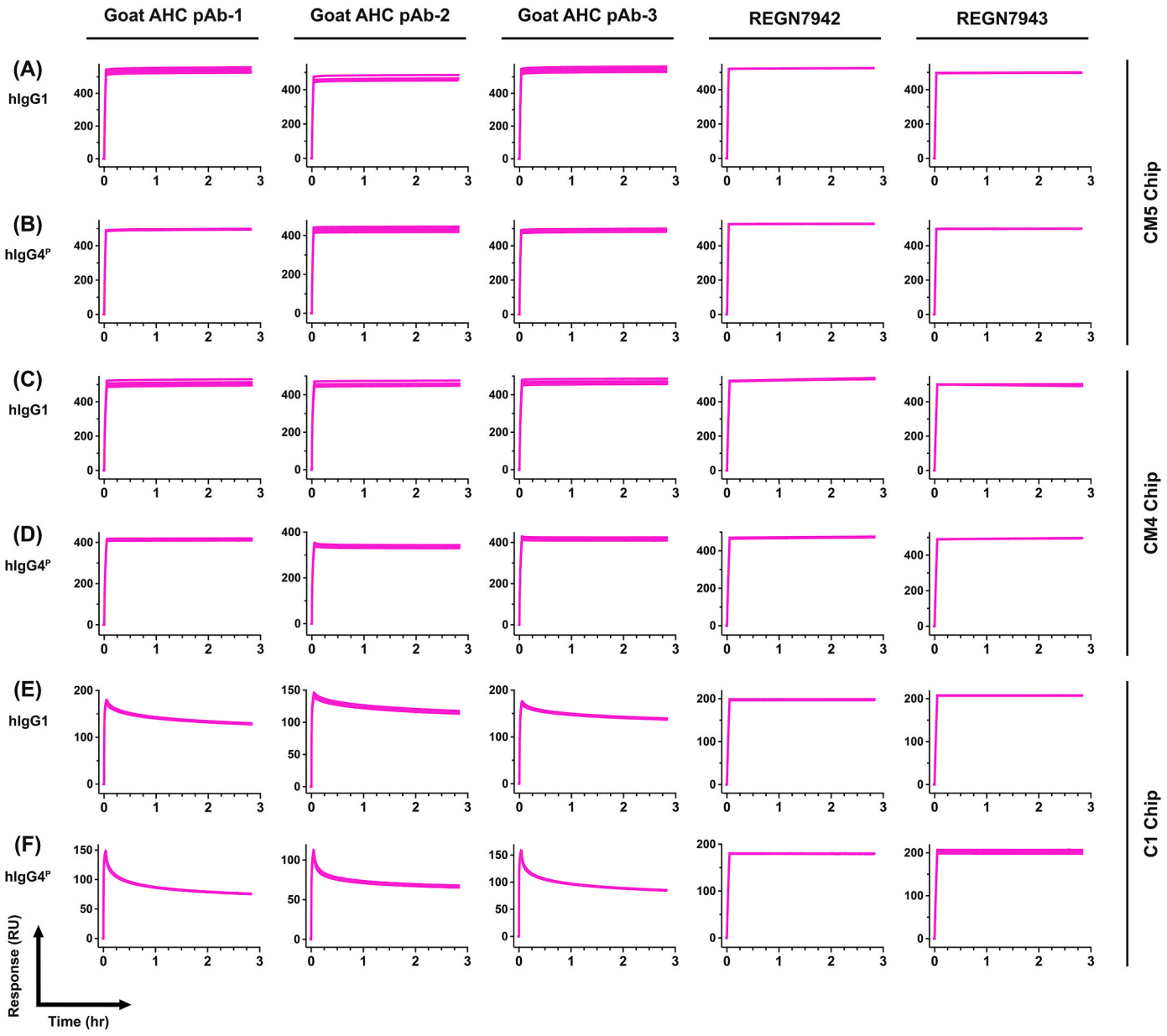

Fig. 9. Binding sensorgrams showing long term stability of hIgG1 or hIgG4^P captured on a CM5, CM4 or C1 sensor chip immobilized with REGN7942, REGN7943 or the three goat AHC pAbs. CM5, CM4 or C1 sensor chips were individually immobilized with REGN7942, REGN7943 or each of the three goat AHC pAbs at a density of approximately 10000–12000 RU, 4000–5000 RU and 1000 RU, respectively. Around 500 RU (CM5 chip), 350–450 RU (CM4 chip) or 100–200 RU (C1 chip) of hIgG1 (**A**, **C**, **E**) or hIgG4^P (**B**, **D**, **F**) were captured on different AHC antibody surfaces and their dissociation in HBS-ET running buffer was monitored for 10,000 s (2 h and 47 min). An overlay of at least triplicate injections of hIgG is shown.

chip to minimize matrix-mediated artifacts [11,40,41]. Additionally, surfaces derivatized with these goat AHC pAbs exhibit a loss in their binding activity following multiple regenerations at physiological temperatures. Although we found that all three goat AHC pAb surfaces reproducibly captured hIgGs at 25°C over multiple regeneration cycles, raising the temperature to 37°C typically dropped capture levels by ~40–50% after 70 regeneration cycles, especially for hmAbs expressed as hIgG4^P (data not shown). To address this limitation, multiple regeneration conditions (different regeneration buffers and/or injection times) were screened but we were unable to identify an optimum condition that retains the binding activity of the goat AHC pAb surfaces at 37°C. The polyclonal nature of these goat AHC antibodies and the inevitable lot-to-lot variability in their binding properties makes it even more challenging to standardize the regeneration condition. We therefore pursued developing a reliable in-house AHC mAb that could be used for performing capture kinetic assays to support the drug discovery of Regeneron Pharmaceuticals. Moreover, since mAbs are clonal, different lots of AHC mAbs are expected to exhibit identical binding properties, resulting in a more consistent results of the capture kinetic assays, irrespective of the lot used.

Several mAb clones binding to hIgG with diverse properties and specificities were generated in-house to develop different immunoassays and the six mouse AHC mAbs used in this study were selected based on their high affinity and binding specificity to the Fc region of different hIgG subclasses (hIgG1, hIgG2, and hIgG4). Extensive binding studies were performed to characterize these six mouse AHC mAbs and their utility as hIgG capture reagents in label-free binding assays was assessed. Our data showed that all six mouse AHC mAbs bind specifically to the Fc region of hIgG with no cross-reactivity to hFab, rabbit IgG, cynomolgus monkey IgG and rhesus monkey IgG. Moreover, they bind

Table 6
List of hmAbs binding to Ag-1 (21.9kD) or Ag-2 (74.7kD) expressed with different hIgG variants.

hmAb #	hIgG Subclass	Ag Details	Details of hIgG Variants	Reference
hmAb-1	hIgG1	Ag-1 (21.9kD)	Wild-type	
hmAb-2			H435R, Y436F	[12]
hmAb-3			E233P, L234V, L235A, del (G236), H268Q, K274Q, Y296F, A327G, A330S, P331S	[25–29, 33]
hmAb-4			N297Q	[34]
hmAb-5			N297D	[34]
hmAb-6	hIgG2		Wild-type	
hmAb-7	hIgG4		Wild-type	
hmAb-8			S228P	[25,26]
hmAb-9			S228P, E233P, F234V, L235A, del(G236)	[25–28]
hmAb-10			E233P, F234V, L235A, del (G236)	[27,28]
hmAb-11			S228P, E233P, F234V, L235A, del(G236), N297Q	[25–28, 34]
hmAb-12			S228P, E233G, F234G, del (L235), M252Y, S254T, T256E	[19, 25–28]
hmAb-13			S228P, E233G, F234G, del (L235)	[25–28]
hmAb-14			S228P, E233P, F234V, L235A, del(G236), H435R, Y436F, L445P	[12, 25–28]
hmAb-15			S228P, E233G, F234G, del (L235) N297Q	[25–28, 34]
hmAb-16	hIgG1	Ag-2 (74.7kD)	M252Y, V308P, N434Y	[17]
hmAb-17			M428L, N434S	[18]
hmAb-18			H433K, N434F	[16]
hmAb-19			H433K, N434F, H435R, Y436F	[12,16]
hmAb-20			M252Y, N286E, N434Y	[17]
hmAb-21			M252Y, N434Y	[17]
hmAb-22			Knob: T366W & Hole: T366S, L368A, Y407V, H435R, Y436F	[12,13]
hmAb-23	hIgG4		S228P	[25,26]
hmAb-24			S228P, M428L, N434S	[18,25,26]
hmAb-25			S228P, H433K, N434F	[16,25,26]
hmAb-26			S228P, H433K, N434F, H435R, Y436F, L445P	[12,16,25, 26]
hmAb-27			S228P, M252Y, N286E, N434Y	[17,25,26]

with high affinity to 43 different hIgG variants; commonly cited in the literature to have modified antibody effector functions and/or PK profile. Different Biacore sensor surfaces individually derivatized with these mouse AHC mAbs on a CM5 chip showed high hIgG binding capacity and are able to stably capture more than 4000 RU with no baseline drift as opposed to the saturation of the three goat AHC pAb surfaces at ~1,500 RU. Moreover, the sensitivity to capture 0.1 μg/mL hIgG on a CM5 chip is comparable between the six mouse AHC mAb and the three goat AHC pAb surfaces. The AHC mAb surfaces reproducibly capture 600–650 RU of hmAbs, even after 300 capture-regeneration cycles. Although all six AHC mAbs exhibit properties of an ideal capture reagent

Table 7
Results of the capture kinetic analyses performed on six representative hmAb-Ag interactions using a CM5 sensor chip individually immobilized with REGN7942, REGN7943 and three goat AHC pAbs.

hmAb #	hIgG Details	Ag Details	Goat AHC pAb-1 Surface				Goat AHC pAb-2 Surface				Goat AHC pAb-3 Surface				REGN7942 Surface				REGN7943 Surface			
			k_a ($M^{-1}s^{-1}$)	k_d (s^{-1})	K_D (nM)	$t_{½}$ (min)	k_a ($M^{-1}s^{-1}$)	k_d (s^{-1})	K_D (nM)	$t_{½}$ (min)	k_a ($M^{-1}s^{-1}$)	k_d (s^{-1})	K_D (nM)	$t_{½}$ (min)	k_a ($M^{-1}s^{-1}$)	k_d (s^{-1})	K_D (nM)	$t_{½}$ (min)	k_a ($M^{-1}s^{-1}$)	k_d (s^{-1})	K_D (nM)	$t_{½}$ (min)
hmAb-1	hIgG1	Ag-1 (21.9kD)	9.07	6.37	0.70	18.1	9.41	6.49	0.69	17.8	9.12	6.24	0.68	18.5	9.36	6.23	0.67	18.5	9.42	6.23	0.66	18.5
hmAb-6	hIgG2		10.47	6.28	0.60	18.4	10.78	6.29	0.58	18.4	9.42	6.21	0.66	18.6	9.80	6.13	0.63	18.8	8.66	6.03	0.70	19.2
hmAb-7	hIgG4		8.64	6.37	0.74	18.1	9.00	6.46	0.72	17.9	8.82	6.38	0.72	18.1	9.65	6.30	0.65	18.3	9.29	6.18	0.67	18.7
hmAb-8	hIgG4p		8.97	6.25	0.70	18.5	9.67	6.39	0.66	18.1	8.67	6.28	0.73	18.4	9.20	6.17	0.67	18.7	9.36	6.13	0.66	18.9
hmAb-23	hIgG4p	Ag-2 (74.7kD)	3.23	3.78	1.17	30.6	3.44	3.93	1.14	29.4	3.11	3.88	1.25	29.8	4.22	4.67	1.11	24.7	4.46	4.59	1.03	25.2
hmAb-16	hIgG1 (M252Y, V308P, N434Y)		3.46	3.96	1.14	29.2	3.75	4.03	1.07	28.7	3.04	3.89	1.28	29.7	4.22	4.82	1.14	24.0	4.44	4.61	1.04	25.0

Values reported in the table are k_a (x 10^5 $M^{-1}s^{-1}$), and k_d (x 10^{-4} s^{-1}).

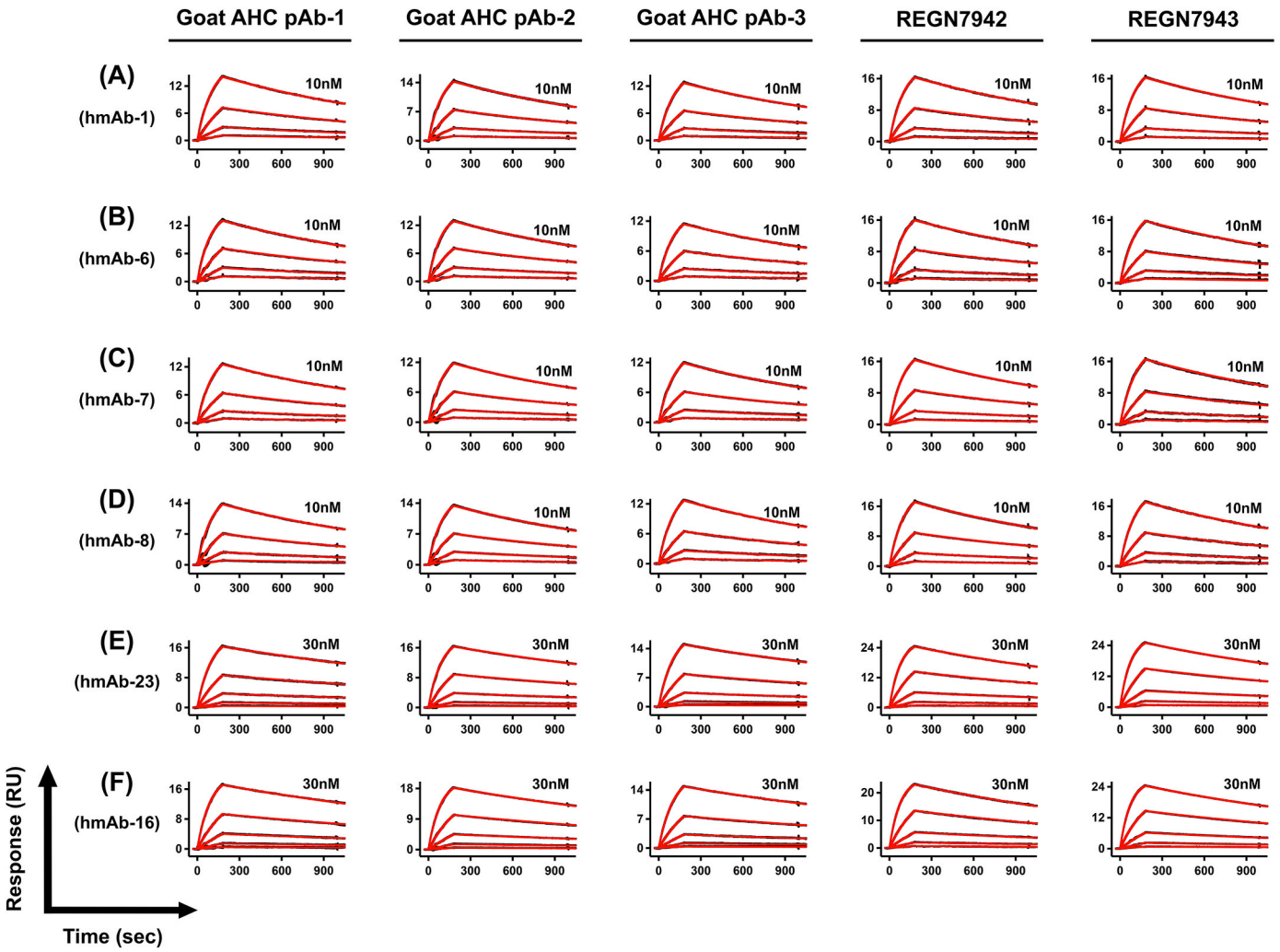

Fig. 10. Capture kinetic analyses performed on hmAb-Ag interactions expressed with canonical hIgG and selective hIgG Fc variantusing three goat AHC pAbs, REGN7942 or REGN7943 immobilized surfaces. Capture kinetic analyses was performed by capturing 90 RU or 35 RU of hmAb binding to (**A**–**D**) 21.9kD Ag or (**E**, **F**) 74.7kD Ag, respectively. The hmAbs, expressed as (**A**) hIgG1, (**B**) hIgG2, (**C**) hIgG4, (**D**, **E**), hIgG4^{P} or (**F**) hIgG1 with M252Y/V308P/N434Y variant were captured over three goat AHC pAbs, REGN7942 or REGN7943 immobilized CM5 sensor surfaces. Different concentrations of respective Ags (serially diluted by three-fold) were later injected for 3 min followed by a 15 min of dissociation time. The real time binding sensorgrams (shown in black) represent duplicate injections for each Ag concentration while the fits generated by globally fitting the data using 1:1 binding model with mass transport limitation are shown as red lines. The highest Ag concentration used to fit the data is shown and Table 7 provides the results of the kinetic analyses. (For interpretation of the references to color in this figure legend, the reader is referred to the Web version of this article.)

for performing kinetic assays on a label-free biosensor, only REGN7942 and REGN7943 were selected for in-depth assessment of their utility as capture reagent to characterize hmAb-Ag interactions due to their overall higher binding affinity to different hIgG variants and longer $t_{½}$ values. In contrast to the goat AHC pAbs, immobilization of REGN7942 or REGN7943 on a CM4 or C1 chip allows stable capture of 500 RU of IgG1 and IgG4^{P} with no drop in the binding response even after 10,000 s (Fig. 9 and Supplementary Fig. 4), further supporting the superiority of REGN7942 and REGN7943 as capture reagents compared to the three commercial goat AHC pAbs. This is an important finding, since it will allow characterization of mAb binding to a wide range of molecular weight Ags, irrespective of the sensor chips used, which would be difficult to achieve using any of the three goat AHC pAbs used in this study.

The binding kinetic parameters for a total of 31 hmAbs, with binding affinities ranging from 40 pM to 1 nM measured using REGN7942 and REGN7943 immobilized surfaces are within two-fold of the values determined using the three goat AHC pAb surfaces. We understand that although a 5% reduction in the binding response was observed, an extended dissociation time would have been preferred to reliably characterize picomolar affinity hmAbs presented in Fig. 11; especially for hmAbs binding to 27.7kD and 57.8kD Ags. Additionally, a solution based binding affinity measurement would be a favored assay to validate the accuracy of the binding kinetic values generated on the SPR platform. We have previously characterized these hmAbs using KinExA and reported that the k_a, k_d, and K_D values determined on Biacore 4000 were within six-fold of the KinExA data [10]. The purpose of including these four picomolar affinity hmAbs again in the current study was to verify if we see any discrepancies in the binding kinetic parameters measured between the three goat AHC pAb, REGN7942 and REGN7943 immobilized surfaces; as previously reported with the commercial mouse AHC mAb [10]. As such, extending the dissociation time for more than an hour would be beyond the scope of the current study.

Characterization of Ag binding to picomolar and sub-picomolar affinity mAbs, especially with the dissociation rate constants of less than 10^{-5} s^{-1}, is typically challenging on a SPR biosensor. Extended dissociation times of 2–4 h are typically required to observe Ag dissociation, which limits the utility of capture kinetics assay to screen such

Table 8
Results of the capture kinetic analyses performed on four different picomolar affinity hmAbs using three goat AHC pAb, REGN7942, and REGN7943 capture surfaces.

Ag Details	Capture Surface	k_a ($M^{-1}s^{-1}$)	k_d (s^{-1})	K_D (pM)	$t_{½}$ (min)
Ag-1 (14.8kD)	Goat AHC pAb-1	4.69	1.97	42.70	586
	Goat AHC pAb-2	4.60	2.20	47.80	525
	Goat AHC pAb-3	4.81	1.96	40.70	589
	REGN7942	4.16	1.96	47.10	589
	REGN7943	4.24	2.02	47.70	572
Ag-2 (17.9kD)	Goat AHC pAb-1	6.54	7.44	113.76	155
	Goat AHC pAb-2	6.44	7.29	113.20	158
	Goat AHC pAb-3	5.49	7.57	137.89	153
	REGN7942	6.00	6.47	107.83	179
	REGN7943	5.79	6.56	113.30	176
Ag-3 (27.7kD)	Goat AHC pAb-1	1.82	0.89	49.40	130
	Goat AHC pAb-2	1.97	1.00	50.70	116
	Goat AHC pAb-3	1.81	0.81	44.20	143
	REGN7942	2.74	1.04	38.10	111
	REGN7943	2.63	0.98	37.20	118
Ag-4 (57.8kD)	Goat AHC pAb-1	1.93	1.20	62.30	963
	Goat AHC pAb-2	2.09	1.20	57.30	963
	Goat AHC pAb-3	1.73	1.10	63.60	1050
	REGN7942	2.43	1.19	49.10	971
	REGN7943	2.45	1.10	45.00	1050

Values reported in the table are k_a (x 10^5 $M^{-1}s^{-1}$), k_d (x 10^{-5} s^{-1}).

picomolar affinity mAbs. The baseline drift caused by the dissociation of captured mAb from the immobilized AHC surface and the experimental long-term noise during such extended dissociation can significantly impact the results of capture kinetic analyses of mAb-Ag interactions. Therefore, researchers prefer performing longer dissociation studies by covalently coupling the mAb to the sensor surface at low densities using different surface chemistries [40]. However, there are multiple challenges with directly coupling the mAb to the sensor surface: (i) mAb coupling is typically performed in acidic pH to allow its pre-concentration into the dextran matrix and can potentially denature or deactivate the mAb, (ii) mAb may attach to the sensor surface in random orientations and in turn can affect Ag binding (iii) requires optimization of regeneration condition for each surface-linked mAb without affecting its binding activity, which can be challenging, (iv) new surfaces need to be derivatized for each mAb which limits the throughput capability and further extends the analysis time. In this embodiment we show that REGN7942 and REGN7943 are better AHC capture reagents than the three commercial goat AHC pAbs included in this study and can stably capture 500 RU of hIgG for 10,000 s without any drop in the capture level even on a C1 sensor chip. We therefore believe that REGN7942 and REGN7943 surfaces can overcome most of the challenges experienced during the characterization of such picomolar affinity interactions and can be routinely used to screen mAbs. However, to reliably characterize picomolar affinity interactions with slow dissociation rates ($k_d < 10^{-5}$ s^{-1}) and/or fast association rates ($k_a > 10^7$ $M^{-1}s^{-1}$), we encourage everyone to adopt orthogonal solution based affinity measurements using the KinExA, GyroLab or Meso Scale Discovery (MSD) platforms, as performed previously [10,42–44]. Data generated using these orthogonal methods will reveal any unexpected inconsistencies in the SPR binding kinetic values and in turn will provide higher confidence in the accuracy of the k_a, k_d and K_D values; especially for picomolar affinity mAbs.

Our data demonstrate that both REGN7942 and REGN7943 are ideal AHC mAbs and can be routinely used to perform capture kinetic analyses on label-free biosensors to characterize mAbs with a wide range of binding affinities. Although the present study was initiated as an internal assay development project to identify the best in-house AHC mAb for mAb screening, we wanted to share our findings with the scientific community and showcase the attributes of an ideal AHC mAb for reliable measurement of k_a, k_d, and K_D values of mAb-Ag interactions on a label-free biosensor. Multiple AHC mAbs are currently available from various commercial vendors and we encourage everyone to adopt some of the assays presented in this study as guidelines for the identification of the

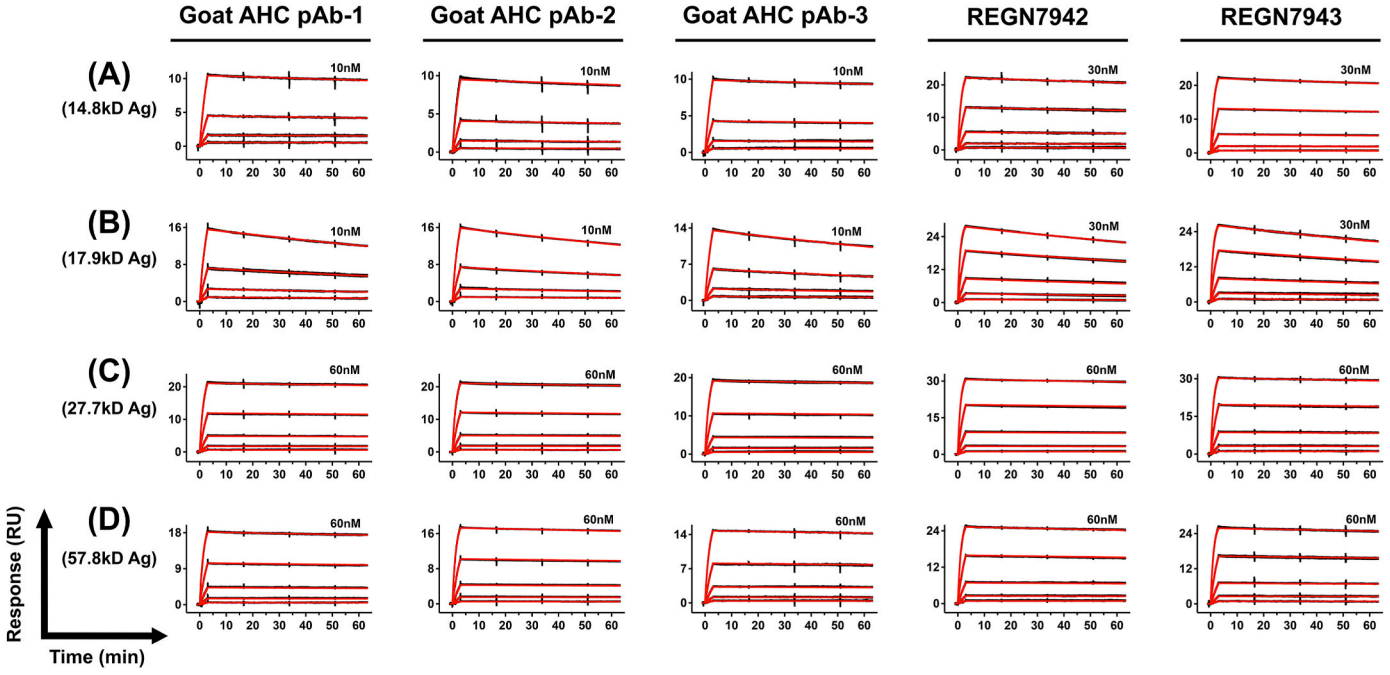

Fig. 11. Capture kinetic analyses performed on four picomolar affinity hmAbs using three goat AHC pAb, REGN7942 or REGN7943 capture surfaces. Similar levels of hmAb binding to (**A**) 14.8kD, (**B**) 17.9kD, (**C**) 27.7kD, or (**D**) 57.8kD Ag were captured over three goat AHC pAb, REGN7942 or REGN7943 immobilized surfaces followed by the injection of different concentrations of their respective Ags (serially diluted by three-fold) for 3 min with an hour of dissociation phase. The real time binding sensorgrams (shown in black) represent at least duplicate injections for each Ag concentration while the fits generated by globally fitting the data using a 1:1 binding model with mass transport limitation is shown as red lines. The highest Ag concentration used to fit the data is provided and the results of the kinetic analyses are provided in Table 7. (For interpretation of the references to color in this figure legend, the reader is referred to the Web version of this article.)

best commercial AHC mAb for performing high throughput capture kinetics assay. We hope our work will provide a benchmark for the identification of appropriate AHC mAb, prior to their use as capture reagents for performing capture kinetic analyses of mAb-Ag interactions.

Reagent availability

Certain Regeneron materials described in this manuscript may be available upon request through our portal (https://regeneron.envisionpharma.com/vt_regeneron/). For any questions about sharing our materials, please connect the preclinical collaborations at preclinical.collaborations@regeneron.com.

Disclosure of potential conflicts of interest

All the authors are employees and shareholders of Regeneron Pharmaceuticals.

CRediT authorship contribution statement

Vishal Kamat: Conceptualization, Investigation, Data curation, Methodology, Writing – original draft, Writing – review & editing. **Candice Boutot:** Methodology. **Ashique Rafique:** Supervision. **Christian Granados:** Methodology. **Jing Wang:** Methodology. **Ashok Badithe:** Methodology. **Marcela Torres:** Methodology. **Ishita Chatterjee:** Methodology. **Olav Olsen:** Conceptualization, Writing – review & editing. **William Olson:** Conceptualization, Writing – review & editing. **Tammy Huang:** Supervision, Writing – review & editing.

Acknowledgements

We are thankful to the team members of Jee-Hae Kim for cloning all the recombinant proteins used in the study. We also appreciate the team members of Raymond Leidich and the preclinical manufacturing and process development (PMPD) for purifying different mAbs, hmAbs and Ags used in the study. Finally, we would like to thank our collaborators at Adimab for developing picomolar affinity hmAb binding to a 14.8kD Ag.

Appendix ASupplementary data

Supplementary data to this article can be found online at https://doi.org/10.1016/j.ab.2021.114455.

References

[1] Q. Zhang, G. Chen, X. Liu, Q. Qian, Monoclonal antibodies as therapeutic agents in oncology and antibody gene therapy, Cell Res. 17 (2007) 89–99.
[2] N. Raje, D.L. Longo, Monoclonal antibodies in multiple myeloma come of age, N. Engl. J. Med. 373 (2015) 1264–1266.
[3] D.M. Ecker, S.D. Jones, H.L. Levine, The therapeutic monoclonal antibody market, mAbs 7 (2015) 9–14.
[4] M.R. Migden, D. Rischin, C.D. Schmults, A. Guminski, A. Hauschild, K.D. Lewis, C. H. Chung, L. Hernandez-Aya, A.M. Lim, A.L.S. Chang, G. Rabinowits, A.A. Thai, L. A. Dunn, B.G.M. Hughes, N.I. Khushalani, B. Modi, D. Schadendorf, B. Gao, F. Seebach, S. Li, J. Li, M. Mathias, J. Booth, K. Mohan, E. Stankevich, H. M. Babiker, I. Brana, M. Gil-Martin, J. Homsi, M.L. Johnson, V. Moreno, J. Niu, T. K. Owonikoko, K.P. Papadopoulos, G.D. Yancopoulos, I. Lowy, M.G. Fury, PD-1 blockade with cemiplimab in advanced cutaneous squamous-cell carcinoma, N. Engl. J. Med. 379 (2018) 341–351.
[5] J.G. Robinson, M. Farnier, M. Krempf, J. Bergeron, G. Luc, M. Averna, E.S. Stroes, G. Langslet, F.J. Raal, M. El Shahawy, M.J. Koren, N.E. Lepor, C. Lorenzato, R. Pordy, U. Chaudhari, J.J.P. Kastelein, Efficacy and safety of alirocumab in reducing lipids and cardiovascular events, N. Engl. J. Med. 372 (2015) 1489–1499.
[6] T.W.J. Huizinga, R.M. Fleischmann, M. Jasson, A.R. Radin, J. van Adelsberg, S. Fiore, X. Huang, G.D. Yancopoulos, N. Stahl, M.C. Genovese, Sarilumab, a fully human monoclonal antibody against IL-6Rα in patients with rheumatoid arthritis and an inadequate response to methotrexate: efficacy and safety results from the randomised SARIL-RA-MOBILITY Part A trial, Ann. Rheum. Dis. 73 (2014) 1626–1634.
[7] D.D. Gladman, P.J. Mease, M.A. Cifaldi, R.J. Perdok, E. Sasso, J. Medich, Adalimumab improves joint-related and skin-related functional impairment in patients with psoriatic arthritis: patient-reported outcomes of the Adalimumab Effectiveness in Psoriatic Arthritis Trial, Ann. Rheum. Dis. 66 (2007) 163–168.
[8] L. Sanchez, Y. Wang, D.S. Siegel, M.L. Wang, Daratumumab: a first-in-class CD38 monoclonal antibody for the treatment of multiple myeloma, J. Hematol. Oncol. 9 (2016) 51.
[9] H. Kaplon, J.M. Reichert, Antibodies to watch in 2021, mAbs 13 (2021) 1860476.
[10] V. Kamat, A. Rafique, T. Huang, O. Olsen, W. Olson, The impact of different human IgG capture molecules on the kinetics analysis of antibody-antigen interaction, Anal. Biochem. 593 (2020) 113580.
[11] G.A. Canziani, S. Klakamp, D.G. Myszka, Kinetic screening of antibodies from crude hybridoma samples using Biacore, Anal. Biochem. 325 (2004) 301–307.
[12] S.J. Davis, E. Smith, D. Macdonald, K.L. Olson, Readily Isolated Bispecific Antibodies with Native Immunoglobulin Format, US Patent 8,586,713. Regeneron Pharmaceuticals, Inc., 2013.
[13] J.B. Ridgway, L.G. Presta, P. Carter, Knobs-into-holes' engineering of antibody CH3 domains for heavy chain heterodimerization, Protein Eng. 9 (1996) 617–621.
[14] I.J. Burvenich, W. Farrugia, F.T. Lee, B. Catimel, Z. Liu, D. Makris, D. Cao, G. J. O'Keefe, M.W. Brechbiel, D. King, V. Spirkoska, L.C. Allan, P.A. Ramsland, A. M. Scott, Cross-species analysis of Fc engineered anti-Lewis-Y human IgG1 variants in human neonatal receptor transgenic mice reveal importance of S254 and Y436 in binding human neonatal Fc receptor, mAbs 8 (2016) 775–786.
[15] R.L. Shields, A.K. Namenuk, K. Hong, Y.G. Meng, J. Rae, J. Briggs, D. Xie, J. Lai, A. Stadlen, B. Li, J.A. Fox, L.G. Presta, High resolution mapping of the binding site on human IgG1 for Fc gamma RI, Fc gamma RII, Fc gamma RIII, and FcRn and design of IgG1 variants with improved binding to the Fc gamma R, J. Biol. Chem. 276 (2001) 6591–6604.
[16] C. Vaccaro, J. Zhou, R.J. Ober, E.S. Ward, Engineering the Fc region of immunoglobulin G to modulate in vivo antibody levels, Nat. Biotechnol. 23 (2005) 1283–1288.
[17] T. Igawa, A. Maeda, K. Haraya, T. Tachibana, Y. Iwayanagi, F. Mimoto, Y. Higuchi, S. Ishii, S. Tamba, N. Hironiwa, K. Nagano, T. Wakabayashi, H. Tsunoda, K. Hattori, Engineered monoclonal antibody with novel antigen-sweeping activity in vivo, PLoS One 8 (2013), e63236.
[18] J. Zalevsky, A.K. Chamberlain, H.M. Horton, S. Karki, I.W. Leung, T.J. Sproule, G. A. Lazar, D.C. Roopenian, J.R. Desjarlais, Enhanced antibody half-life improves in vivo activity, Nat. Biotechnol. 28 (2010) 157–159.
[19] W.F. Dall'Acqua, P.A. Kiener, H. Wu, Properties of human IgG1s engineered for enhanced binding to the neonatal Fc receptor (FcRn), J. Biol. Chem. 281 (2006) 23514–23524.
[20] A.C. Gregory Lazar, Wei Dang, John Desjarlais, Doberstein Stephen, Robert Hayes, Sher Karki, Omid Vafa Optimized Fc Variants and Methods for Their Generation, US Patent 10/672,280 Xencor, Inc., 2004.
[21] G.L. Moore, C. Bautista, E. Pong, D.H. Nguyen, J. Jacinto, A. Eivazi, U.S. Muchhal, S. Karki, S.Y. Chu, G.A. Lazar, A novel bispecific antibody format enables simultaneous bivalent and monovalent co-engagement of distinct target antigens, mAbs 3 (2011) 546–557.
[22] J. Lund, N. Takahashi, J.D. Pound, M. Goodall, R. Jefferis, Multiple interactions of IgG with its core oligosaccharide can modulate recognition by complement and human Fc gamma receptor I and influence the synthesis of its oligosaccharide chains, J. Immunol. 157 (1996) 4963–4969.
[23] M. Hezareh, A.J. Hessell, R.C. Jensen, J.G. van de Winkel, P.W. Parren, Effector function activities of a panel of mutants of a broadly neutralizing antibody against human immunodeficiency virus type 1, J. Virol. 75 (2001) 12161–12168.
[24] S.Y. Chu, I. Vostiar, S. Karki, G.L. Moore, G.A. Lazar, E. Pong, P.F. Joyce, D. E. Szymkowski, J.R. Desjarlais, Inhibition of B cell receptor-mediated activation of primary human B cells by coengagement of CD19 and FcgammaRIIb with Fc-engineered antibodies, Mol. Immunol. 45 (2008) 3926–3933.
[25] J. Schuurman, G.J. Perdok, A.D. Gorter, R.C. Aalberse, The inter-heavy chain disulfide bonds of IgG4 are in equilibrium with intra-chain disulfide bonds, Mol. Immunol. 38 (2001) 1–8.
[26] S. Angal, D.J. King, M.W. Bodmer, A. Turner, A.D. Lawson, G. Roberts, B. Pedley, J. R. Adair, A single amino acid substitution abolishes the heterogeneity of chimeric mouse/human (IgG4) antibody, Mol. Immunol. 30 (1993) 105–108.
[27] S. Davis, E. Smith, S. Patel, A. Rafique, Antibodies Comprising Chimeric Constant Domains, 2014. U.S. Patent, WO/2014/121087.
[28] S. Davis, E. Smith, T. Zhang, S. Patel, Heavy Chain Constant Regions with Reduced Binding to Fc Gamma Receptors, 2016. U.S. Patent, WO/2016/161010 A3.
[29] D.P. Humphreys, S.J. Peters, Polymeric Fc Proteins and Methods of Screening to Alter Their Functional Characteristics, 2018. U.S. Patent, US/2018/0044416 A1.
[30] G.L. Moore, H. Chen, S. Karki, G.A. Lazar, Engineered Fc variant antibodies with enhanced ability to recruit complement and mediate effector functions, mAbs 2 (2010) 181–189.
[31] G.A. Lazar, W. Dang, S. Karki, O. Vafa, J.S. Peng, L. Hyun, C. Chan, H.S. Chung, A. Eivazi, S.C. Yoder, J. Vielmetter, D.F. Carmichael, R.J. Hayes, B.I. Dahiyat, Engineered antibody Fc variants with enhanced effector function, Proc. Natl. Acad. Sci. U. S. A. 103 (2006) 4005–4010.
[32] R. Jefferis, Recombinant antibody therapeutics: the impact of glycosylation on mechanisms of action, Trends Pharmacol. Sci. 30 (2009) 356–362.
[33] O. Vafa, G.L. Gilliland, R.J. Brezski, B. Strake, T. Wilkinson, E.R. Lacy, B. Scallon, A. Teplyakov, T.J. Malia, W.R. Strohl, An engineered Fc variant of an IgG eliminates all immune effector functions via structural perturbations, Methods 65 (2014) 114–126.

[34] S.L. Sazinsky, R.G. Ott, N.W. Silver, B. Tidor, J.V. Ravetch, K.D. Wittrup, Aglycosylated immunoglobulin G1 variants productively engage activating Fc receptors, Proc. Natl. Acad. Sci. U. S. A. 105 (2008) 20167–20172.
[35] R.L. Shields, J. Lai, R. Keck, L.Y. O'Connell, K. Hong, Y.G. Meng, S.H. Weikert, L. G. Presta, Lack of fucose on human IgG1 N-linked oligosaccharide improves binding to human Fcgamma RIII and antibody-dependent cellular toxicity, J. Biol. Chem. 277 (2002) 26733–26740.
[36] J.O. Richards, S. Karki, G.A. Lazar, H. Chen, W. Dang, J.R. Desjarlais, Optimization of antibody binding to FcγRIIa enhances macrophage phagocytosis of tumor cells, Mol. Cancer Therapeut. 7 (2008) 2517–2527.
[37] A. Tammen, S. Derer, R. Schwanbeck, T. Rosner, A. Kretschmer, F.J. Beurskens, J. Schuurman, P.W. Parren, T. Valerius, Monoclonal antibodies against epidermal growth factor receptor acquire an ability to kill tumor cells through complement activation by mutations that selectively facilitate the hexamerization of IgG on opsonized cells, J. Immunol. 198 (2017) 1585–1594.
[38] T.F. Rowley, S.J. Peters, M. Aylott, R. Griffin, N.L. Davies, L.J. Healy, R.M. Cutler, A. Eddleston, T.L. Pither, J.M. Sopp, O. Zaccheo, G. Fossati, K. Cain, A.M. Ventom, H. Hailu, E.J. Ward, J. Sherington, F.R. Brennan, F. Fallah-Arani, D.P. Humphreys, Engineered hexavalent Fc proteins with enhanced Fc-gamma receptor avidity provide insights into immune-complex interactions, Commun Biol 1 (2018) 146.
[39] Z. An, G. Forrest, R. Moore, M. Cukan, P. Haytko, L. Huang, S. Vitelli, J.Z. Zhao, P. Lu, J. Hua, C.R. Gibson, B.R. Harvey, D. Montgomery, D. Zaller, F. Wang, W. Strohl, IgG2m4, an engineered antibody isotype with reduced Fc function, mAbs 1 (2009) 572–579.
[40] A.W. Drake, M.L. Tang, G.A. Papalia, G. Landes, M. Haak-Frendscho, S.L. Klakamp, Biacore surface matrix effects on the binding kinetics and affinity of an antigen/antibody complex, Anal. Biochem. 429 (2012) 58–69.
[41] M.E. Pope, M.V. Soste, B.A. Eyford, N.L. Anderson, T.W. Pearson, Anti-peptide antibody screening: selection of high affinity monoclonal reagents by a refined surface plasmon resonance technique, J. Immunol. Methods 341 (2009) 86–96.
[42] H. Salimi-Moosavi, P. Rathanaswami, S. Rajendran, M. Toupikov, J. Hill, Rapid affinity measurement of protein-protein interactions in a microfluidic platform, Anal. Biochem. 426 (2012) 134–141.
[43] Z. Dai, J. Juneja, L. Schneeweis, D. Cohen, F. Marsilio, P. Morin, R. DasGupta, Application of the Gyrolab microfluidic platform to measure picomolar affinity of a PD-L1-binding Adnectin radioligand for positron emission tomography, Biotechniques 69 (2020) 200–205.
[44] P. Estep, F. Reid, C. Nauman, Y. Liu, T. Sun, J. Sun, Y. Xu, High throughput solution-based measurement of antibody-antigen affinity and epitope binning, mAbs 5 (2013) 270–278.